A Novel Self-Assembled Epitope Peptide Nanoemulsion Vaccine with Targeting the Nasal Mucosal Epithelial Cell for Reinvigorating CD8+ T cell Immune Activity and Inhibiting Tumor Progression

Hongwu Sun (sunhongwu2001@163.com)
Third Military Medical University https://orcid.org/0000-0002-4318-8424
Yun Yang
Third Military Medical University: Army Medical University
Shuang Ge
Third Military Medical University: Army Medical University
Zhen Song
Third Military Medical University: Army Medical University
Anni Zhao
Third Military Medical University: Army Medical University
Liqun Zhao
Third Military Medical University: Army Medical University
Zhiming Hu
Third Military Medical University: Army Medical University
DingYi Cai
Third Military Medical University: Army Medical University
Zelong Zhang
Third Military Medical University: Army Medical University
Liusheng Peng
Third Military Medical University: Army Medical University
Dongshui Lu
Third Military Medical University: Army Medical University
Ping Luo
Third Military Medical University: Army Medical University
Weijun Zhang
Third Military Medical University: Army Medical University
Quanming Zou
Third Military Medical University: Army Medical University

Hao Zeng
Third Military Medical University: Army Medical University

Research

Keywords: Epitope, nanovaccine, CTL, nasal immunization, tumor immunotherapy

Posted Date: November 19th, 2020

DOI: https://doi.org/10.21203/rs.3.rs-108084/v1

Abstract

Synthetic epitope peptide are not suitable for nasal administration due to its weak immunogenic and low delivery efficiency. In this work, we developed a intranasal epitope nanovaccine (I-OVA NE) which can prolong mucosal retention and enhance CTL activity induced by epitopes. I-OVA NE was a nanoemulsion system that assembled with IKVAV-$OVA_{257-264}$(I-OVA) conjugated peptides.This nanovaccine with I-OVA at a concentration of 4 mg/mL showed the average particle size of 30.37±2.49 nm, zeta potential of -16.67±1.76 mV, and encapsulation rate of 84.07±7.59%. I-OVA NE particles exhibit smooth and spherical surfaces, good dispersibility and no obvious aggregation. Moreover, the physicochemical characteristics (size, PdI and zeta potential) of this vaccine did not significantly change in the condition of mucin exist. I-OVA NE had no significant cytotoxic effects on BEAS-2B cells, and no obvious acute pathological changes were observed on nasal mucosa or lung tissue in the mice after nasal immunization. We found that I-OVA NE prolonged the nasal residence time, promoted the cellular uptake of the epitope peptide and improved the antigen uptake efficiency of BEAS-2B cells, but this effect was significantly decreased after integrin blockade. Importantly, the level of Th1 cytokines and the proportion of epitope-specific CD8+ T cells increased significantly, and thus I-OVA NE protected E.G7/OVA tumor-bearing mice by suppressing tumour growth and provoking anti-tumour immune activation. Overall, these data indicate that I-OVA NE can be an applicable strategy for tumor vaccine design.

1. Introduction

Tumors are the second leading cause of death worldwide, with approximately 15% of patients dying every year. In 2018, nearly 609,640 patients died of tumors in the USA. It is estimated that by 2030, an excess of 20 million newly diagnosed people and 13 million related deaths from tumors will occur each year[1, 2].In the past 30 years, tumor vaccines have been widely studied in animal models. Current, the USA FDA has approved only one of prostate tumor vaccine (Sipuleucel-T) for the treatment of prostate tumors with metastatic castration resistance in patients with limited symptoms[3].Recently, a kind of vaccine was produced by encapsulating OVA protein chemically modified with MPG ΔNLS (MPG ΔNLS–OVA conjugate) in poly (lactide-co-glycolide) acid nanoparticles. These results showed that that vaccine assisted the escape of antigens from lysosomes into the cytosol, increase the amount of antigens processed in the cytosol, and subsequently enhance antigen cross-presentation via MHC-I molecules to elicit cytotoxic CD8 + T cell responses[3]. However, there are no reports of OVA epitope peptides chemically modified with other chemicals among tumor vaccines.

A desired tumor vaccine can stimulate strong adaptive immune response to tumor antigens. Epitope peptide vaccines have become potential candidate methods for tumor immunotherapy. Compared with traditional vaccines, this type of vaccine has the advantages of high specificity, safety and convenient production, especially some MHC restricted epitope can induce potent CTL activity to eliminate tumor cell and be prepared personalized based on the variation of tumor antigens, so it has attracted increasing attention in tumor vaccine research[4]. Epitope vaccines have many advantages, including drug delivery,

fate control, cell targeting, deep tumor tissue penetration, and improved treatment efficacy of tumors, and they have become unique and promising tumor treatment tools[5].

Epitope peptide vaccines can stimulate specific T cells in tumor patients to play an effective role in immune-protective therapy. The recruitment of T cells can destroy and clear tumor cells quickly to prevent the occurrence of tumors. An important reason for tumor escape from immune surveillance is the downregulation of tumor-specific T cells[6]. T cells, especially CD8 + cytotoxic T cells, are the most effective components for recognizing changes in transformed cells, and CD8 + T cell vaccines have become a new paradigm in the development of tumor vaccines[7].

Moreover, nasal administration is an effective and safe method of tumor vaccine administration because of convenience, the avoidance of parenteral administration and improved patient compliance. IKVAV is a core pentapeptide of laminin which is a binding peptide of integrin. Human respiratory epithelial cells normally express α3 and β1 integrin, so the binding of IKVAV to integrin may enhance antigen uptake of nasal mucosal epithelial cell[8, 9].

Recent studies of antitumor epitope vaccines in both animal models and clinics have achieved no satisfactory anti-tumor effect for the following reasons: (1) peptide epitope do not have enough immunogenicity; (2) the lack of delivery efficiency may be due to the rapid degradation of extracellular peptides, which diffuse rapidly from the administration site so that insufficient antigen uptake by immune cells [10, 11]. At the same time, the epitope peptide is easily to diffused and degraded at the administration site, resulting in failure to activate an effective T cell response[6]. The epitope peptide vaccine must be treated with antigen-presenting cells (APCs) and activate T cells (primitive CD4 + T cells and CD8 + T cells) in lymph nodes. Activated T helper cells (Th cells) and cytotoxic T lymphocytes need to infiltrate the tumor site to transform the immunosuppressive tumor microenvironment to the proinflammatory environment and exert antitumor effects [12]. Adjuvants used in combination with tumor vaccines have complementary patterns of action on immune cells [13].

To overcome the shortcomings of nasal epitope vaccine, we developed a intranasal epitope nanovaccine (I-OVA NE), a nanoemulsion system that assembled with IKVAV-$OVA_{257-264}$ (I-OVA) conjugated peptides, as shown in Fig. 1. The physicochemical characteristics and stability, toxicity, uptake and release profiles were studied *in vivo* and *in vitro*. The vaccine-induced immune response and tumor cells elimination were investigated. Furthermore, the protective and therapeutic effects induced by I-OVA NE were tested by E.G7/OVA tumor-bearing mice model.

2. Results

2.1 Synthetic peptide conjugation of IKVAV and $OVA_{257-264}$

Amine groups on the surface were used to conjugate IKVAV the $OVA_{257-264}$ peptide via reduction in a two step-process. We were able to conjugate IKVAV and peptide at a similar ratio of approximately 1:5. The

HPLC and MS of $OVA_{257-264,}$ IKVAV and IKVAV-$OVA_{257-264}$ are shown in Figure S1-S6. These data confirmed successful IKVAV-$OVA_{257-264}$ coupling.

2.2 Effects of different peptide concentrations on nanovaccines

The effects of the OVA257-264 and I-OVA concentrations in the the nanoemulsion vaccine on the size, polydispersity index, zeta potential, and encapsulation efficacy are shown in Figure S7A-D and Fig. 2A-Figure 2D. Figure S7A and Fig. 2A show that the average size positively correlated with OVA 257–264 and I-OVA concentration (from 0 to 8000 μg/ml) but suddenly decreased to 22.61 ± 0.71 nm and 30.37 ± 2.49 nm at 4000 μg/ml ($P < 0.001$; $P < 0.001$). These data showed that the PdI changed from 0.195 ± 0.02 to 0.137 ± 0.042 at 4000 μg/ml ($P > 0.05$, $P < 0.05$)(Fig. 2B & S7B). The zeta potentials of OVA NE and I-OVA NE changed from − 35 to -12 mV and − 35 to -11 mV (0-8000 μg/ml), respectively, but there was a significant difference when the concentration was 4000 μg/ml ($P < 0.05$; $P < 0.05$) (Fig. 2C & S7C). Importantly, as shown in Figure S7D and Fig. 2D, these results showed that as the concentration increased from 1000 μg/ml to 8000 μg/ml, the encapsulation efficiency of these nanoemulsion vaccines increased from 80–95% and from 70–84% ($P < 0.05$; $P < 0.05$). At concentrations up to 4000 μg/ml, the encapsulation rate was highest, at 95 ± 2.41% and 84.07 ± 7.59%. Therefore, we chose 4000 μg/ml I-OVA as the optimal load concentrations.

2.3 Preparation, characterization and stability of I-OVA NE

The nanoemulsion vaccine is a clear and bright liquid. These results showed that the droplets size of I-OVA NE were 20.0 nm on average, almost entirely less than 100 nm, and results in no droplets accumulation, as shown in Fig. 2E. As shown in Fig. 2F, the AFM images show that most of the droplets are spherical, with an average diameter of approximately 20 nm, ranges from 10 nm to 60 nm. Figure 2G shows that the average particle size of this novel I-OVA NE is 229.33 ± 2.82 nm, with a narrow distribution range. Figure 2H shows that the zeta potential of this vaccine is -16.67 ± 1.76 mV. The nanoemulsion vaccines of OVA and I-OVA were stable without obvious aggregation in mucin solution.

2.4 Cytotoxicity and *in vivo* toxicity of I-OVA NE

The cytotoxicity of BNE, I-OVA, BNE + I-OVA, and I-OVA NE in BEAS-2B cells was determined by a CCK 8 Kit after treatment for 24 h. We found that BEAS-2B cell survival ratios for the I-OVA NE vaccine administered at 0.5, 1, 2, 4 and 8 mg/mL were 97.71 ± 0.76%, 98.04 ± 1.17%, 98.7 ± 0.83%, 96.8 ± 1.38% and 98.6 ± 0.66%, respectively. These results indicate that I-OVA NE had no obvious cytotoxicity to BEAS-2B cells (Figure S8). In addition, as histological examination showed in Fig. 3, the lungs of the PBS group mice had no significant cell infiltration in the alveolar and interstitial spaces of the tissues. In the I-OVA NE group, there was slight cell infiltration in the lung, but the alveolar structure was intact. In the nasal cavities of mice, there was no destruction of the nasal mucosal structure and were no inflammatory pathological changes in each group. That is, there was no obvious inflammatory cell infiltration, bleeding or tissue damage were observed in the lung and nasal mucosa.

2.5 BEAS-2BCellular Uptake of the I-OVA NE

We found that more nanoemulsions of FTIC-labeled I-OVA was captured by epithelial BEAS-2B cells than by the water solution, as shown in Fig. 4A. The cellular uptake rates of I-OVA NE (68.83 ± 5.45%) were higher than those of I-OVA (14.44 ± 9.47%) ($P < 0.001$) and the BNE control (1.19 ± 0.64%), as shown in Fig. 4B. Therefore, we found that this I-OVA NE greatly improved the uptake efficiency of the epitope peptide in BEAS-2B cells.

2.6 Antibody-blocking effect of I-OVA NE

As in the I-OVA NE group, the proportions of FITC + BEAS-2B cells after treatment with PBS, isotype control and integrin blocked were 66.68 ± 4.64%, 66.47 ± 2.67%, and 54.87 ± 3.27%, respectively. Figure 4C shows that the proportion of I-OVA NE was higher than that of FITC + BEAS-2B cells treated with PBS. Isotype-controlled and integrin-blocked cells were 18.81 ± 3.40%, 19.96 ± 6.64% and 19.49 ± 7.79%, respectively ($P < 0.001$; $P < 0.0001$; $P < 0.001$). The proportion of FITC + BEAS-2B cells of I-OVA NE in the integrin antibody blocking group was obviously lower than in the PBS control group and isotype groups ($P < 0.01$).

2.7 *In vivo* nasal release of I-OVA NE

It is important to determine whether this vaccine delays nasal release *in vivo*. We found that I-OVA NE had a delayed release effect compared to the water solution of I-OVA, as shown in Fig. 5A. The ratio of the relative average florescence intensity of I-OVA NE compared to its solution significantly maintained the release effect (Fig. 5B). Additionally, we found that even 12 h after nasal administration, the fluorescence intensity was higher than that obtained in aqueous solution at 6 h. At the same time, the results showed that the slow-release effect of I-OVA NE at 0.5 h and 6 h was significantly better than that of I-OVA ($P < 0.01$ and $P < 0.05$). Therefore, we think that I-OVA NE can prolong the sustained time, delay rapid release in the nasal area and improve the cellular uptake of peptides. The results showed that the nanoemulsion vaccine had high vaccine delivery efficiency.

2.8 Antigen specificity of the antibody response of I-OVA NE

The antigen specificity of the antibody response is an important characteristic of acquired immune humoral immunity and is also a key aspect of vaccines that plays a role in specific immune protection mechanisms. These data showed that five kinds of antibodies in the serum of IgG, IgG1, IgG2a, IgG2b or IgA antibodies had equal levels, and there was no significant difference ($P > 0.05$; $P > 0.05$; $P > 0.05$; $P > 0.05$; $P > 0.05$) between the groups, as shown in Figure S10A-Figure S10F.

2.9 Cytokine levels effect I-OVA NE

The detection of cytokine levels is necessary to determine the immune response of the I-OVA NE vaccine. The Bio-Plex Pro Mouse Cytokine 23-plex Assay results for cerebral and cerebellar concentrations are shown in Fig. 6A. In this study, we found that this vaccine can greatly improve the T-helper (Th) 1 immune

response, including the levels of IL-1α, IL-1β, IL-2, IL-3, IL-12p40, IL12p70, IL-13, eotaxin, GM-CSF, IFN-γ, MIP-1b, RANTES and TNF-α, compared to I-OVA (all $P < 0.05$), except for G-CSF ($P > 0.05$), CXCR1 (KC) ($P > 0.05$), MCP ($P > 0.05$), and MIP-1a ($P > 0.05$), as shown in Figure S11A-Figure S11Q and Fig. 6B. Additionally, I-OVA NE stimulated an increase or decrease in Th2 (IL-4, IL-5, IL-6, IL-9, IL-10) and Th17 cytokine IL-17A levels compared to I-OVA (all $P < 0.05$), as shown in Figure S12A-Figure S12F and Fig. 6C. Therefore, this vaccine can activate and enhance cellular (Th1/Th17) and humoral immune responses (Th2) in the body after intranasal immunization.

2.10 Specific CD8 + T levels of I-OVA NE

Whether I-OVA NE could induce a strong cellular immune response and immune memory is a key question? We found that, In Fig. 7A, the proportions of antigen-specific CD8 + T cells after treatment with PBS, BNE, I-OVA, BNE + I-OVA and I-OVA NE were 0.11 ± 0.09%, 0.09 ± 0.02%, 0.28 ± 0.22%, 0.62 ± 0.39% and 1.25 ± 0.68%, respectively. The proportion in the I-OVA group and the BNE + I-OVA group was slightly higher than that in the PBS and BNE control groups. The ratio in the I-OVA NE group was significantly higher than that in the I-OVA group ($P < 0.01$), indicating that the I-OVA NE group could induce a strong cellular immune response and memory after immunization. These data suggested that the administration of I-OVA NE after immunization can induce a strong cellular immune response and immune memory.

2.11 In vitro CTL response of I-OVA NE

Lower proportions of $CFSE^{high}$ cells indicated greater clearance of E.G7 cells, suggesting a stronger tumor killing ability of the CTL response. As shown in Fig. 7B and Fig. 7C, the proportions of $CFSE^{high}$ cells in the PBS, BNE, I-OVA, BNE + I-OVA and I-OVA NE groups were 100.1 ± 3.79%, 93.49 ± 2.75%, 105.5 ± 4.52%, 85.43 ± 4.98% and 58.61 ± 5.27%, respectively. The proportion in the I-OVA NE group was significantly lower than those in the I-OVA and BNE + I-OVA groups ($P < 0.001$). These results showed that CTL activity can be induced by immunization at sufficient levels to kill peptide-presenting tumor cells, suggesting that the immune response can effectively inhibit tumor growth.

2.12 Preventive protection effect of I-OVA NE

We investigated whether passive immunization with I-OVA NE was protective. In the I-OVA NE and BNE + I-OVA groups, the tumors grew with a significant delay compared with those in the PBS group ($P < 0.05$, $P < 0.001$). In the 18-day I-OVA NE group, the tumor volume was significantly smaller than that in the I-OVA group ($P < 0.001$), as shown in Fig. 8A-Figure 8C. The results showed that the I-OVA NE group had better preventive immune protection than the other groups. The median survival times of the PBS group, BNE group, I-OVA group, BNE + I-OVA group and I-OVA NE group were 18, 18, 18, 22.5 and 28.5 days, respectively. The median survival time was significantly different between the I-OVA NE and I-OVA groups ($P < 0.001$). Additionally, the median survival time of the I-OVA group was shorter than that of the BNE + I-OVA group ($P < 0.05$). These results proved that the I-OVA NE vaccine had a better preventive protection effect than the other groups.

2.13 Therapeutic protective effect of I-OVA NE

As shown in Fig. 8D-Figure 8E, in the 18-day I-OVA NE group, the tumor volume was significantly smaller than that in the I-OVA group ($P < 0.001$). These results indicated that the I-OVA NE group had a better therapeutic effect than the other groups. The median survival times of the PBS group, BNE group, I-OVA group, BNE + I-OVA group and I-OVA NE group were 18, 18, 18, 22.5 and 27 days, respectively. The median survival time was significantly different between the I-OVA NE and I-OVA groups ($P < 0.01$). Additionally, the median survival time of the I-OVA group was shorter than that of the BNE + I-OVA group ($P < 0.05$). It was proven that the I-OVA NE vaccine had a better therapeutic effect than the other groups.

3. Discussion

In 2019, there were 174,650 new diagnoses of tumors and 31,620 deaths in the USA [14]. Tumor vaccines use tumor antigens with appropriate adjuvants to activate a patient's adaptive immune response and eliminate tumor cells. It is well known that CD8 + T cells play an important role in tumor inhibition[15]. Cytotoxic CD8 + T cells can release molecules such as perforin, granzyme, lymphotoxin, interferon and tumor necrosis factor to induce tumor cell lysis or apoptosis. Cytotoxic CD8 + T cells can also bind to the death receptor Fas on tumor cells through FasL on the surface of CD8 + T cells, activating the death signal transduction pathway and directly killing tumor cells[16]. After maturation, dendritic cells migrate to draining lymph nodes and present processed protein antigens to CD8 + T cells in the form of linear peptide epitopes through major histocompatibility complex (MHC) class I and class II molecules to initiate an appropriate immune response to antigens[17]. Additionally, CD8 + T cells kill tumor cells through the immune response of MHC class I endogenous-derived antigens and shuttle vaccine particles through endocytosis for cross presentation[18]. In recent years, traditional tumor vaccines have rarely been successful in clinical trials due to their poor immunogenicity and limited safety. Numerous studies have shown that nanomaterial tumor vaccines elicit a more durable and effective immune response than conventional vaccines[19]. It has been reported that the PC7A nanoparticle vaccine can significantly reduce tumor growth inhibition and improve the survival rate in TC-1 and B16-OVA tumor-bearing mice [20]. Studies have shown that the nanovaccine can induce strong antigen-specific cell immunity to B16-OVA melanoma, playing a significant preventive role. More importantly, when the nanovaccine was used in combination with the apoptotic process 1 checkpoint to block immunotherapy, it showed good efficiency against B16-OVA melanoma [21]. The above studies showed that the efficiency of nanovaccines in penetrating the lymphatic vessels to reach and aggregate in the lymph nodes was significantly correlated with the size, and nanoparticles smaller than 50 nm were more likely to target the lymph nodes. The preparation of 10–50 nm nanoscale tumor vaccines based on this approach is particularly important[22]. Therefore, in this study, a novel nanovaccine with a size of less than 50 nm was designed and prepared as the coupling peptide of IKVAV and $OVA_{257-264}$ (CD8 + T cell peptide).

Adjuvant is very important to ideal tumor vaccine. Many reporter think that a kind of O/W MF59 adjuvant could been used in the tumor vaccine. But, MF59 was not an ideal adjuvant for mucosal immunity due to its large particle size and poor antigen loading [23, 24]. Because it is an oil in a water emulsion system

with large particles, mainly suitable for loading fat soluble drugs or antigens, and its loading capacity for water-soluble antigen peptides is unsatisfactory[24, 25]. Some reported it may enhance the levels of various chemokines in inflamed areas and to promote the aggregation of monocytes, macrophages and DC cells to promoting antigen presentation and enhancing the specific immune response[26–29]. Therefore, we design the O/W formulate similar to the MF59 emulsion adjuvant.

Moreover, hydrophilic $OVA_{257-264}$ was coupled with IKVAV modified by palmitic acid to increase the partial amphiphilic property of the conjugated molecules. Our results also showed that changes in the drug loading of I-OVA influenced the particle size of the nanoemulsions. The particle size of the I-OVA NE vaccine decreased to 30.37 ± 2.49 nm when the drug loading was 4 mg/ml. Therefore, we believe that the I-OVA peptide is not only an antigenic component loaded by nanoemulsions but also participates in the formation of nanoemulsions vaccines and promotes the stability of vaccine and mucosal immune responses.

The basic characteristics of size, pdI, zeta potential and electrophoretic mobility did not change after the addition of 0.05 mg/ml mucins, as shown in Figure S7. These results show that I-OVA NE possessed good stability and revealed good physical and chemical characteristics. Mucous on the surface of nasal mucosa contains large amounts mucin, which is a kind of mucopolysaccharide. It has the functions of lubrication, moisturizing and forming a chemical barrier to the surface of the nasal mucosa. Mucins can interact with antigens or delivery systems to cause aggregation and "capture" antigens, reducing the delivery efficiency of vaccine proteins [22, 30]. In addition, mucin is involved in the formation of the mucus layer on the surface of the mucosa. The mucus layer is essentially a gel, and its microstructure is a cross-linked network structure. Particles smaller than 300 nm can pass through, while particles of 20–40 nm can pass more easily[22]. Therefore, the study of mucin is particularly important for the stability of vaccines. In this study, we found that I-OVA NE vaccines did not interact to cause aggregation after adding the mucin.

Additionally, the loading of the epitope peptide delivery system is the key to improving the transfer efficiency. The uptake efficiency of BEAS-2B cells for I-OVA NE had the expected effect. IKVAV enhanced the adhesion of respiratory tract epithelial cells to nanoemulsions, which could enhance the transmission of epitopes. It is also very important to prove the binding of IKVAV to integrin. Additional, we found that the uptake rate of I-OVA NE by BEAS-2B cells was still higher than that of I-OVA, indicating that nanoemulsion was also a key factor in promoting the uptake of antigen by epithelial cells. There was no difference in the media with and without nonimmune IgG antibody ($P > 0.05$) in the I-OVA group. These results indicated that the conjugation of IKVAV and OVA257-264 enhanced the uptake of I-OVA by BEAS-2B cells through IKVAV bonded to integrin.

At the same time, we blocked integrin α3, α6 and β1 subunit by corresponding monoclonal antibody. We found that blocking BEAS-2B by integrin had no effect on the uptake of OVA, but the I-OVA uptake rate was decreased significantly (Fig. 4C). This result suggested that the combination of IKVAV and integrin mucosal epithelial cells in the nanoemulsion drug delivery system was significantly increased. However,

after blocking by integrin, the uptake rate of BEAS-2B to the nanoemulsion vaccine was still higher than that of free I-OVA, which indicated that the nanoemulsion itself was an important factor in improving delivery efficiency in addition to IKVAV. Therefore, this novel nanovaccine has good delivery and uptake efficacy when administered nasally.

In this study, we found that I-OVA, a CD8 + T cell epitope, theoretically does not cause a specific antibody response. The immune specificity of the antibody in mouse serum was consistent with that in the PBS, BNE, I-OVA, BNE + I-OVA and I-OVA NE groups, and the serum IgG, IgG1, IgG2a, IgG2b and IgA levels were consistent. We also found that I-OVA NE stimulated an increase or decrease in Th2 (IL-4, IL-5, IL-6, IL-9, IL-10) and Th17 cytokine IL-17A levels compared to I-OVA (all $P < 0.05$), as shown in Figure S12A-Figure S12F and Fig. 6C. These data suggest that nanoemulsion vaccines can play a role in improving the immune response of Th1/Th2/Th17 cells.

The tumor cell line of E. G was derived from EL4 lymphoma cells. The plasmid carried an intact chicken OVA gene and neomycin (G418) resistance gene, which led to the synthesis and secretion of that peptide[31]. Toll-like receptor 4 (TLR4) agonists have a long history in the field of tumor immunotherapy. To date, only two TLR4 agonist adjuvants (BCG and MPLA) have been approved by the FDA for clinical application in tumor treatment [32]. It has been reported that the application of MPL in liposome vaccine can promote the immune peptide-induced CTL response to tumor cells, significantly improving the production of IFN-γ and the activity of CTLs[33]. The same concentration of 0.5 μM CFSE-labeled um participant T cells ($CFSE^{low}$) was added for internal interaction. The larger the proportion of $CFSE^{high}$ cells was, the lower the clearance rate, and the stronger the CTL response. Therefore, we added MPL to the nanovaccine, and these results showed that I-OVA NE could inhibit the growth of tumors. Half of the mice survived 30 days after transplantation, and the rest died approximately 21 days after transplantation. In contrast to the preventive effect, the key to the therapeutic effect is to quickly trigger a strong specific immune response because immune memory has not been induced before[34]. The results showed that I-OVA NE immunization could effectively inhibit tumor growth and prolong the median survival time of mice.

4. Conclusion

In this study, a nanovaccine loaded IKVAV conjugated with a MHC restricted epitope peptide of OVA($OVA_{257-264}$) showed good stability and had no significant toxic effects on BEAS-2B cells, mouse nasal mucosa or mouse lung tissue after nasal administration. Additionally, this vaccine remarkably improved the antigen uptake efficiency of BEAS-2B, but this effect was significantly decreased after integrin blockade. Overall, these data indicate that this nanovaccine targeting CD8 + T cell may be used as an effective tumor vaccine to increase the uptake efficacy and delay the release ratio of antigens *in vitro* and *in vivo*, and increasing the amount of CTLs induced by immunization led to the effective killing and clearance of E.G7 cells. This study provides a practical nanovaccine delivery system for the construction of an innovation platform in immunotherapy by inducing an immune response.

5. Experimental Section

Cell lines, peptide and animal

BEAS-2B epithelial cells from human bronchi were purchased from the ATCC and cultured in RPMI 1640 medium containing 10% fetal bovine serum (FBS). Mouse lymphocyte E.G7 cells from EL 4 were purchased from the ATCC and cultured in 90% RPMI 1640 medium with 2 mM L-glutamine adjusted to contain 1.5 g/L sodium bicarbonate, 4.5 g/L glucose, 10 mM HEPES and 1.0 mM sodium pyruvate and supplemented with 0.05 mM 2-mercaptoethanol and 0.4 mg/ml G418, and10% fetal bovine serum. C57BL/6 mice (6–8 weeks, SPF, female) and nude mice (6–8 weeks, SPF, female) were purchased from Beijing HFK Biotechnology Limited Company (Beijing, China). Animal experiments were carried out on the basis of the handbook for the use and care of experimental animals and approved by the Animal Care and Use Committee of the TMMU of the Chinese PLA. Synthetic peptide conjugation of IKVAV and $OVA_{257-264}$(I-OVA) is produced by Shanghai Botai Biotechology Co.,Ltd.(Shanghai,China). All mice that underwent surgery were treated with sodium pentobarbital anaesthesia to minimize suffering.

Determine the optimal drug load of the epitope peptide vacccine

The oil phase (SQ), the surfactant (Tween 80), and the cosurfactant (IKVAV), water was used as the aqueous phase according to a previously reported method[35]. Five different concentrations (0, 1000, 2000, 4000, and 8000 μg/ml) of $OVA_{257-264}$ and I-OVA, and their nanoemulsions vaccines (OVA NE and I-OVA NE) were designed and prepared. The average size, polydispersity indexes, and zeta potential of these vaccines were measured using a NANO ZS instrument. The encapsulation efficacy and drug load were also measured by an E2695 HPLC (USA) with a C18 column (5 μm, 4.6 mm × 250 mm) at a wavelength of 220 nm.

Preparation of the I-OVA NE nanovaccine: Tween80 and IKVAV were mixed at a mass ratio of 25:1[36]. Then, the mixture of I-OVA (4000 μg/ml) and MPLA (1000 μg/ml) was prepared by low-energy emulsification agitation methods after the addition of squalene (7:3, Smix/squalene). The same method was used in the BNE control (blank emulsion), replacing water with the epitope peptide.

Morphological, physicochemical and stability characteristics of I-OVA NE: The morphology and molecular structure were observed by a JEM-1230 TEM in the JEOL Limited Company of Japan and IPC-208 in Chong Qing University after the samples were diluted with water (1:200)[36]. Additionally, the distribution of size and zeta potential were obtained by a Malvern NANO ZS dynamic light scattering particle size potential meter. In addition, OVA NE (4 mg/ml) and I-OVA NE (4 mg/ml) were diluted 200 times with ultrapure water or mucin (0.05 mg/ml), and a Nano ZS dynamic light scattering particle size potential meter was used to detect particle size, pdI, zeta potential and electrophoresis mobility at 25℃.

In vitro and *in vivo* toxicity assays

The toxicity of I-OVA, I-OVA NE and BNE in BEAS-2B cells was measured using CCK-8 Kits (Dojingdo, Japan) 10 μl I-OVA, BNE + I-OVA, I-OVA NE with 0.5 to 8 mg/ml concentration, BNE as a control, and BEAS-2B cells (10^4 cells/well) were then incubated at 37 ℃ for 24 h. Cell viability was measured by a BioRad reader at 450 nm after the addition of CCK8[37]. Nasal immunization of C57BL/6 mice with 10 μl in each nostril continued for 3 days of I-OVA, BNE + I-OVA and I-OVA NE at a concentration of 4 mg/mL I-OVA, PBS and BNE as the control. The nasal and lung tissues were fixed with 4% paraformaldehyde for 24 h and embedded in paraffin after all mice were euthanized. The toxicity, including hyperemia, edema, neutrophil infiltration, and structural damage in the nasal mucosa tissue and lung tissue, was observed after samples were stained with hematoxylin and eosin.

Antigen uptake by BEAS-2B cells

BEAS-2B cells (5×10^5 cells/well) were cultured overnight at 37 °C in 12-well plates with coverslips. Then, 100 μl of FITC-labeled I-OVA NE or I-OVA (4 mg/ml I-OVA) was added and placed at 37℃ for 90 min. BNE was used as the control. The samples were fixed with 4% paraformaldehyde for 20 min in the dark after washing three times with 0.1M PBS.The cellular uptake values were obtained by an LSM800 CLSM from the Zeiss Limited Company of Germany after staining with DAPI (Life Technologies Limited Company, USA).

Integrin antibody blocking study

The cell was discard the original medium,and add 1 ml of fresh complete medium to each well.The blocking group was added with a final concentration of 50ug/mL Abcam anti integrin antibody α3, α1 and β1.The control medium contained purified normal mouse IgG antibodies at a final concentration of 150 μg/ml.Then, 100 μl of FITC-labeled I-OVA NE or I-OVA (both 4 mg/ml I-OVA) was added and placed at 37℃ for 90 min.PBS was used as the control. After the cells were digested with trypsin, Cells positive for FITC were measured by a FACS Verse of BD Limited Company, USA[38].

In vivo release of I-OVA NE vaccine

Nude mice were intranasally administered 10 μl of 4 mg/ml PE-labeled I-OVA, I-OVA NE, or water in each nostril. All mice were anesthetized with isoflurane gas at 0, 0.5, 1.5, 3, 6, 9, 12 and 24 h and captured by the IVIS system (Caliper Life Science Limited Company). The radiance data and live images of all mice were handled with Living Image software (Ver. 4.4).

Immunization and serum sample collection

C57BL/6 mice were intranasally immunized in each nostril with 10 μl of I-OVA, BNE + I-OVA, I-OVA NE (all 4 mg/ml I-OVA), PBS as the negative control on days 0, 7 and 14. One week after the last immunization, Serum was collected from the mice and stored at -80 °C until further analysis.

ELISA for specific immune response antibodies: Serum samples (1:50, primary antibodies) were added to precoated 96-well plates containing 10 μg/well $OVA_{257-264}$ and placed at 37 °C for 60 min. Then, 1:5000

HRP-conjugated goat anti-mouse antibodies against IgG, IgG1, IgG2a IgG2b and IgA (Bethy, Santa Cruz, CA, USA) were added and incubated at 37 °C for 40 min. These OD values were measured by a BioRad reader at 450 nm.

Cytokine level of splenocyte stimulation

Splenocytes (5×10^6 cells/well) were isolated from immunized mouse spleens and suspended in RPMI 1640 medium with 10% fetal bovine serum. These cells were incubated at 37 °C with 10 μg/ml $OVA_{257-264}$ for 96 h. The cytokine levels of the Th1 immune response (IL-1α, IL-1β, IL-2, IL-3, IL-12p40, IL12p70, IL-13, eotaxin, G-CSF, GM-CSF, IFN-γ, CXCR1 (KC), MCP, MIP-1a, MIP-1b, RANTES and TNF-α), Th2 (IL-4, IL-5, IL-6, IL-9, IL-10), and Th17 (IL-17A) were determined using the Bio-Plex Pro Mouse Cytokine Grp I Panel 23-plex liquid-phase suspension microarray (Bio-Rad). The assay was conducted according to the manufacturer's protocol, with each sample analyzed in duplicate. For washing steps, a Bio-Plex Handheld Magnetic Washer (Bio Rad, USA) was used. A Luminex 200™ system (Luminex Corporation, The Netherlands) was used for the detection and quantification of analytes. Data were processed with Bio-Plex Manager software (version 6.1, Bio Rad, USA).

CD8 + T cell immune response

To quantitatively determine the specific I-OVA ratio of CD8 + T cells, splenocytes (5×10^6 cells/well) were isolated from immunized mouse spleens and suspended in RF-10 medium. These cells were incubated at 37 °C with a final concentration 10 μg/ml $OVA_{257-264}$ for 96 h and stained with the tetramer of H-2Kb OVA (MBL, Japan) for 30 min in the dark. The CD8 + T cell numbers were determined with FACS Verse Flow cytometry.

In vitro CTL assay

One week after the above immunization, splenocytes (1×10^7 cells/well) were mixed with 1×10^5 $CFSE^{high}$ E.G7 cells (E.G7 with 5 μM CFSE) and incubated at 37 °C for 24 h. As an internal reference for the mixture of 1×10^5 $CFSE^{low}$ E.G7 cells (E.G7 with 0.5 μM CFSE) and splenocytes (1×10^7 cells), all splenocyte cells were measured by FACS Verse Flow cytometry[38].

In vivo antitumor efficacy of I-OVA NE

C57BL/6 mice were anesthetized with isoflurane (RWD, Life Science company) and subcutaneously injected with E.G7 suspension at a concentration of 5×10^5 cells. In a prophylactic exam, C57BL/6 mice were intranasally immunized in each nostril with 10 μl of BNE, I-OVA, BNE + I-OVA, I-OVA NE, and PBS as the negative control, on days 0, 7 and 14. All mice were challenged with E.G7 tumor cells at 21 days. Tumor volume and percentage of survival were determined over time, and the mice were monitored for 6, 9, 12, 15, and 18 days. In a therapeutic exam, all mice were intranasally immunized with the same immune dose and procedure as in the prophylactic setting, but after infection with E.G7 cells. Tumor volume and survival percentage were measured. For humane reasons, the mice were killed if the tumor

exceeded 3000 mm^3 in size. The formula for the calculation of tumor volume is Volume = $\pi/6 \times L \times W^2$, where W is the tumor width and L is the tumor length [39–42].

Statistical analysis: GraphPad Prism 6.0 was used for the statistical analysis. The differences between the two groups were analyzed by unpaired two tailed *t*-test. One-way ANOVA and Tukey's multiple comparison test were used to analyze the differences among the groups. The survival rate was compared with the log-rank (Mantel-Cox) test. All the values were expressed as the mean ± standard deviation, and the differences were significant, labeled as follows: * $P < 0.05$, * * $P < 0.01$ and * * $P < 0.001$.

Declarations

5. **Acknowledgments**

This study was supported by No. 31670938, 32070924 of National Natural Science Foundation Program of China, No.2014jcyjA0107 and No. 2019jcyjA-msxmx0159 of Natural Science Foundation Project Program of Chongqing.

6. **Disclosure**

The authors report there is no interest conflicts in this study.

References

1. Briquez, P. S.; Hauert, S.; de Titta, A.; Gray, L. T.; Alpar, A. T.; Swartz, M. A.; Hubbell, J. A., *Front Bioeng Biotechnol* **2020,** *8*, 19. DOI 10.3389/fbioe.2020.00019.
2. Siegel, R. L.; Miller, K. D.; Jemal, A., *CA Cancer J Clin* **2018,** *68* (1), 7-30. DOI 10.3322/caac.21442.
3. Maeng, H. M.; Berzofsky, J. A., *F1000Res* **2019,** *8*. DOI 10.12688/f1000research.18693.1.
4. Lei, Y.; Zhao, F.; Shao, J.; Li, Y.; Li, S.; Chang, H.; Zhang, Y., *PeerJ* **2019,** *6*, e6185. DOI 10.7717/peerj.6185.
5. Zhang, L.; Huang, Y.; Lindstrom, A. R.; Lin, T. Y.; Lam, K. S.; Li, Y., *Theranostics* **2019,** *9* (25), 7807-7825. DOI 10.7150/thno.37194.
6. Malonis, R. J.; Lai, J. R.; Vergnolle, O., *Chem Rev* **2020,** *120* (6), 3210-3229. DOI 10.1021/acs.chemrev.9b00472.
7. Fruh, K.; Picker, L., *Curr Opin Immunol* **2017,** *47*, 52-56. DOI 10.1016/j.coi.2017.06.010.
8. Grassme, H.; Henry, B.; Ziobro, R.; Becker, K. A.; Riethmuller, J.; Gardner, A.; Seitz, A. P.; Steinmann, J.; Lang, S.; Ward, C.; Schuchman, E. H.; Caldwell, C. C.; Kamler, M.; Edwards, M. J.; Brodlie, M.; Gulbins, E., *Cell Host Microbe* **2017,** *21* (6), 707-718 e8. DOI 10.1016/j.chom.2017.05.001.
9. Kikkawa, Y.; Hozumi, K.; Katagiri, F.; Nomizu, M.; Kleinman, H. K.; Koblinski, J. E., *Cell Adhes Migr* **2013,** *7* (1), 150-159. DOI 10.4161/cam.22827.

10. Khong, H.; Volmari, A.; Sharma, M.; Dai, Z.; Imo, C. S.; Hailemichael, Y.; Singh, M.; Moore, D. T.; Xiao, Z.; Huang, X. F.; Horvath, T. D.; Hawke, D. H.; Overwijk, W. W., *J Immunol* **2018,** *200* (10), 3464-3474. DOI 10.4049/jimmunol.1700467.
11. Rad-Malekshahi, M.; Fransen, M. F.; Krawczyk, M.; Mansourian, M.; Bourajjaj, M.; Chen, J.; Ossendorp, F.; Hennink, W. E.; Mastrobattista, E.; Amidi, M., *Mol Pharm* **2017,** *14* (5), 1482-1493. DOI 10.1021/acs.molpharmaceut.6b01003.
12. Zhang, R.; Billingsley, M. M.; Mitchell, M. J., *J Control Release* **2018,** *292*, 256-276. DOI 10.1016/j.jconrel.2018.10.008.
13. Bowen, W. S.; Svrivastava, A. K.; Batra, L.; Barsoumian, H.; Shirwan, H., *Expert Rev Vaccines* **2018,** *17* (3), 207-215. DOI 10.1080/14760584.2018.1434000.
14. Parenky, A. C.; Akalkotkar, A.; Mulla, N. S.; D'Souza, M. J., *Vaccine* **2019,** *37* (41), 6085-6092. DOI 10.1016/j.vaccine.2019.08.033.
15. Peng, M.; Mo, Y.; Wang, Y.; Wu, P.; Zhang, Y.; Xiong, F.; Guo, C.; Wu, X.; Li, Y.; Li, X.; Li, G.; Xiong, W.; Zeng, Z., *Mol Cancer* **2019,** *18* (1), 128. DOI 10.1186/s12943-019-1055-6.
16. van Montfoort, N.; Borst, L.; Korrer, M. J.; Sluijter, M.; Marijt, K. A.; Santegoets, S. J.; van Ham, V. J.; Ehsan, I.; Charoentong, P.; Andre, P.; Wagtmann, N.; Welters, M. J. P.; Kim, Y. J.; Piersma, S. J.; van der Burg, S. H.; van Hall, T., *Cell* **2018,** *175* (7), 1744-1755 e15. DOI 10.1016/j.cell.2018.10.028.
17. Duinkerken, S.; Horrevorts, S. K.; Kalay, H.; Ambrosini, M.; Rutte, L.; de Gruijl, T. D.; Garcia-Vallejo, J. J.; van Kooyk, Y., *Theranostics* **2019,** *9* (20), 5797-5809. DOI 10.7150/thno.35059.
18. Guan, X.; Chen, J.; Hu, Y.; Lin, L.; Sun, P.; Tian, H.; Chen, X., *Biomaterials* **2018,** *171*, 198-206. DOI 10.1016/j.biomaterials.2018.04.039.
19. Vijayan, V.; Mohapatra, A.; Uthaman, S.; Park, I. K., *Pharmaceutics* **2019,** *11* (10). DOI 10.3390/pharmaceutics11100534.
20. Luo, M.; Liu, Z.; Zhang, X.; Han, C.; Samandi, L. Z.; Dong, C.; Sumer, B. D.; Lea, J.; Fu, Y. X.; Gao, J., *J Control Release* **2019,** *300*, 154-160. DOI 10.1016/j.jconrel.2019.02.036.
21. Xu, J.; Wang, H.; Xu, L.; Chao, Y.; Wang, C.; Han, X.; Dong, Z.; Chang, H.; Peng, R.; Cheng, Y.; Liu, Z., *Biomaterials* **2019,** *207*, 1-9. DOI 10.1016/j.biomaterials.2019.03.037.
22. Lai, S. K.; Wang, Y. Y.; Hanes, J., *Adv Drug Deliv Rev* **2009,** *61* (2), 158-71. DOI 10.1016/j.addr.2008.11.002.
23. Ren, S. T.; Zhang, X. M.; Sun, P. F.; Sun, L. J.; Guo, X.; Tian, T.; Zhang, J.; Guo, Q. Y.; Li, X.; Guo, L. J.; Che, J.; Wang, B.; Zhang, H., *PLoS One* **2017,** *12* (1), e0169501. DOI 10.1371/journal.pone.0169501.
24. Yang, L. Y.; Zhou, H.; Yang, Y.; Tong, Y. N.; Peng, L. S.; Zhu, B. H.; Diao, W. B.; Zeng, H.; Sun, H. W.; Zou, Q. M., *Rsc Adv* **2018,** *8* (18), 9996-10008. DOI 10.1039/c7ra13630g.
25. Reddy, L. H.; Couvreur, P., *Adv Drug Deliv Rev* **2009,** *61* (15), 1412-26. DOI 10.1016/j.addr.2009.09.005.
26. Calabro, S.; Tortoli, M.; Baudner, B. C.; Pacitto, A.; Cortese, M.; O'Hagan, D. T.; De Gregorio, E.; Seubert, A.; Wack, A., *Vaccine* **2011,** *29* (9), 1812-23. DOI 10.1016/j.vaccine.2010.12.090.

27. Mosca, F.; Tritto, E.; Muzzi, A.; Monaci, E.; Bagnoli, F.; Iavarone, C.; O'Hagan, D.; Rappuoli, R.; De Gregorio, E., *Proc Natl Acad Sci U S A* **2008,** *105* (30), 10501-6. DOI 10.1073/pnas.0804699105.
28. O'Hagan, D. T.; Ott, G. S.; Nest, G. V.; Rappuoli, R.; Giudice, G. D., *Expert Rev Vaccines* **2013,** *12* (1), 13-30. DOI 10.1586/erv.12.140.
29. Seubert, A.; Monaci, E.; Pizza, M.; O'Hagan, D. T.; Wack, A., *J Immunol* **2008,** *180* (8), 5402-12. DOI 10.4049/jimmunol.180.8.5402.
30. Wong, P. T.; Wang, S. H.; Ciotti, S.; Makidon, P. E.; Smith, D. M.; Fan, Y.; Schuler, C. F. t.; Baker, J. R., Jr., *Mol Pharm* **2014,** *11* (2), 531-44. DOI 10.1021/mp4005029.
31. Huang, Y.; Zou, Y.; Lin, L.; Zheng, R., *DNA Cell Biol* **2017,** *36* (12), 1168-1177. DOI 10.1089/dna.2017.3923.
32. Shetab Boushehri, M. A.; Lamprecht, A., *Mol Pharm* **2018,** *15* (11), 4777-4800. DOI 10.1021/acs.molpharmaceut.8b00691.
33. Vollmer, J.; Krieg, A. M., *Adv Drug Deliv Rev* **2009,** *61* (3), 195-204. DOI 10.1016/j.addr.2008.12.008.
34. Patel, A.; Kaufman, H. L.; Disis, M. L., *Chin Clin Oncol* **2017,** *6* (2), 19. DOI 10.21037/cco.2017.02.04.
35. Sun, H.; Liu, K.; Liu, W.; Wang, W.; Guo, C.; Tang, B.; Gu, J.; Zhang, J.; Li, H.; Mao, X.; Zou, Q.; Zeng, H., *Int J Nanomedicine* **2012,** *7*, 5529-43. DOI 10.2147/IJN.S36071.
36. Sun, H.; Wei, C.; Liu, B.; Jing, H.; Feng, Q.; Tong, Y.; Yang, Y.; Yang, L.; Zuo, Q.; Zhang, Y.; Zou, Q.; Zeng, H., *Int J Nanomedicine* **2015,** *10*, 7275-90. DOI 10.2147/IJN.S91529.
37. Yang, Y.; Chen, L.; Sun, H. W.; Guo, H.; Song, Z.; You, Y.; Yang, L. Y.; Tong, Y. N.; Gao, J. N.; Zeng, H.; Yang, W. C.; Zou, Q. M., *J Nanobiotechnol* **2019,** *17*. DOI ARTN 6 10.1186/s12951-019-0441-y.
38. Desai, A.; Geraghty, S.; Dean, D., *J Biomech* **2019,** *82*, 337-345. DOI 10.1016/j.jbiomech.2018.11.004.
39. Fujita, T.; Teramoto, K.; Ozaki, Y.; Hanaoka, J.; Tezuka, N.; Itoh, Y.; Asai, T.; Fujino, S.; Kontani, K.; Ogasawara, K., *Cancer Res* **2009,** *69* (12), 5142-50. DOI 10.1158/0008-5472.CAN-08-2499.
40. Jeanbart, L.; Ballester, M.; de Titta, A.; Corthesy, P.; Romero, P.; Hubbell, J. A.; Swartz, M. A., *Cancer Immunol Res* **2014,** *2* (5), 436-47. DOI 10.1158/2326-6066.CIR-14-0019-T.
41. Penafuerte, C.; Ng, S.; Bautista-Lopez, N.; Birman, E.; Forner, K.; Galipeau, J., *Cancer Res* **2012,** *72* (5), 1210-20. DOI 10.1158/0008-5472.CAN-11-1659.
42. Yuba, E.; Kono, Y.; Harada, A.; Yokoyama, S.; Arai, M.; Kubo, K.; Kono, K., *Biomaterials* **2013,** *34* (22), 5711-21. DOI 10.1016/j.biomaterials.2013.04.007.

Figures

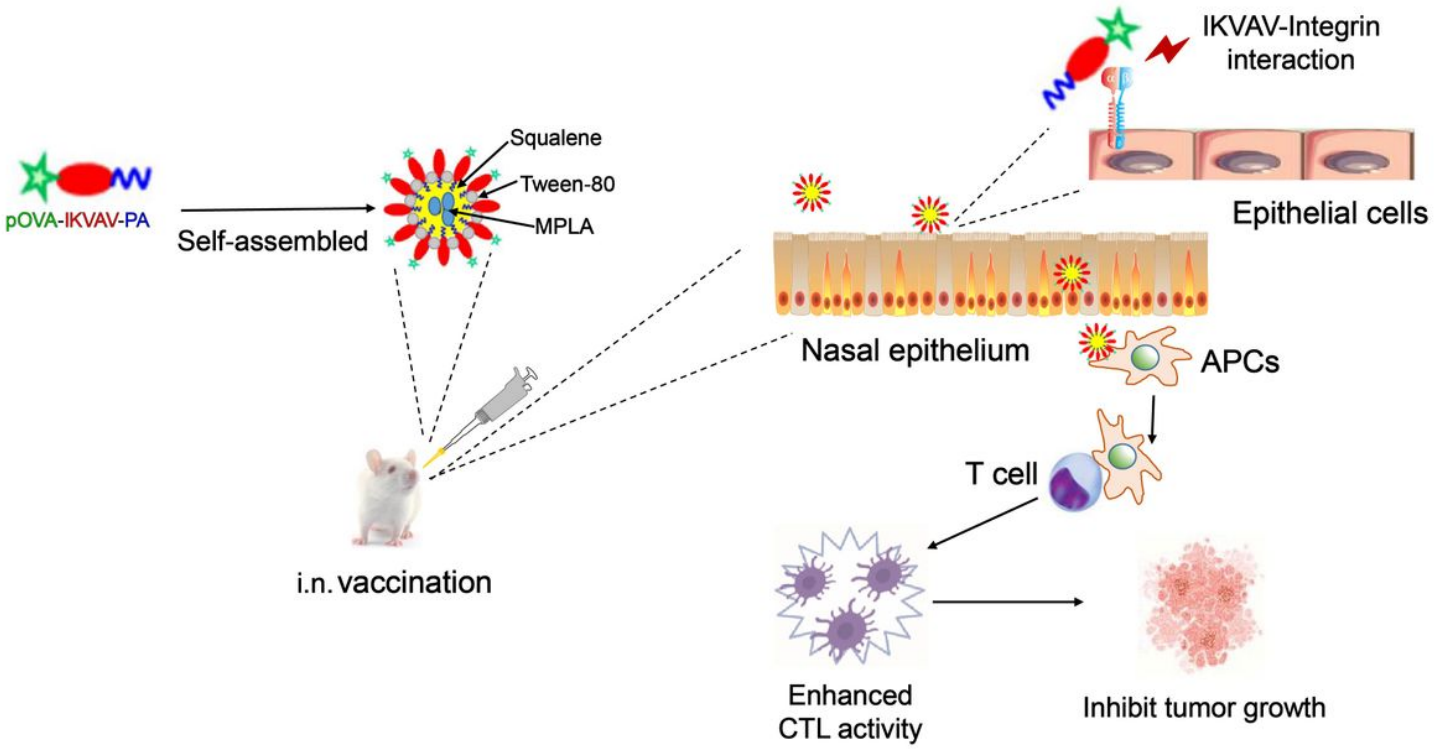

Figure 1

Design and schematic illustration of the proposed mode of action for this novel I-OVA NE vaccine.

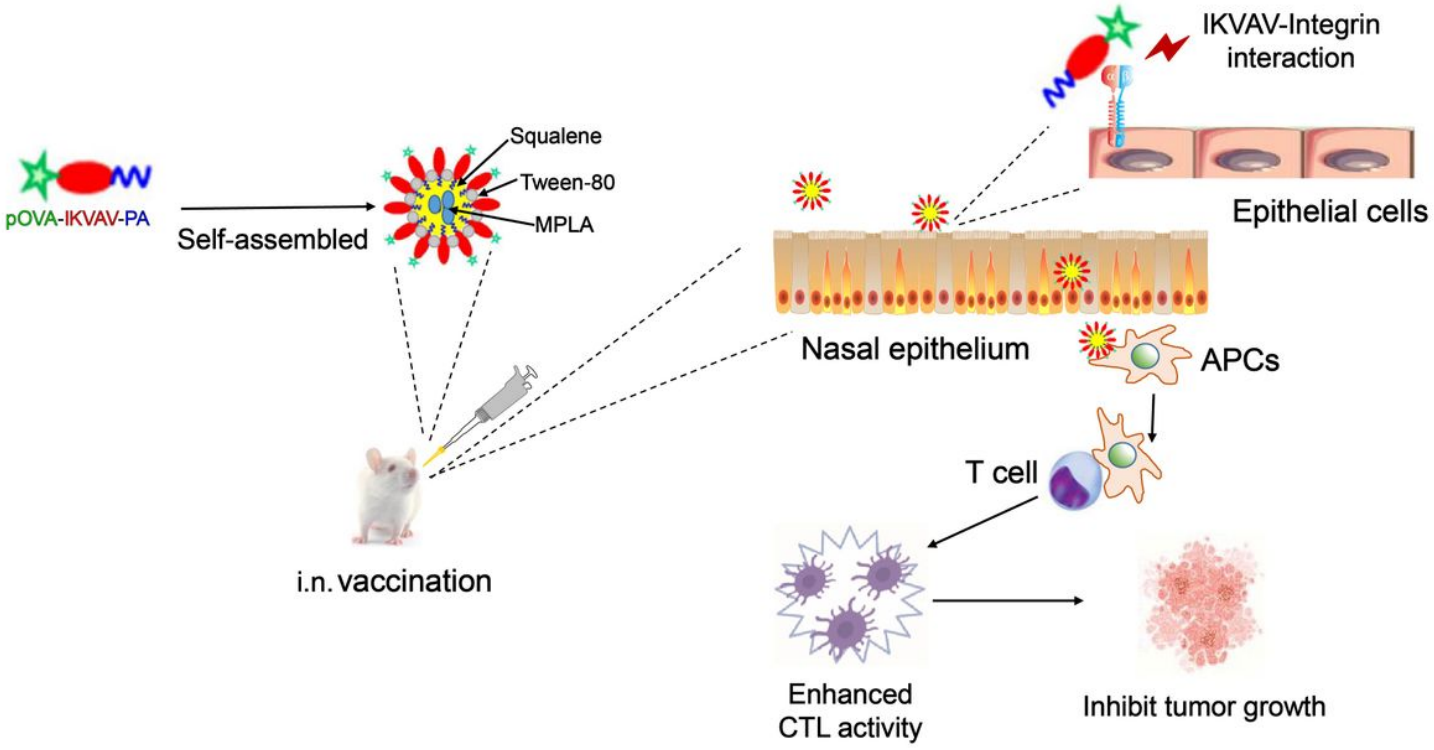

Figure 1

Design and schematic illustration of the proposed mode of action for this novel I-OVA NE vaccine.

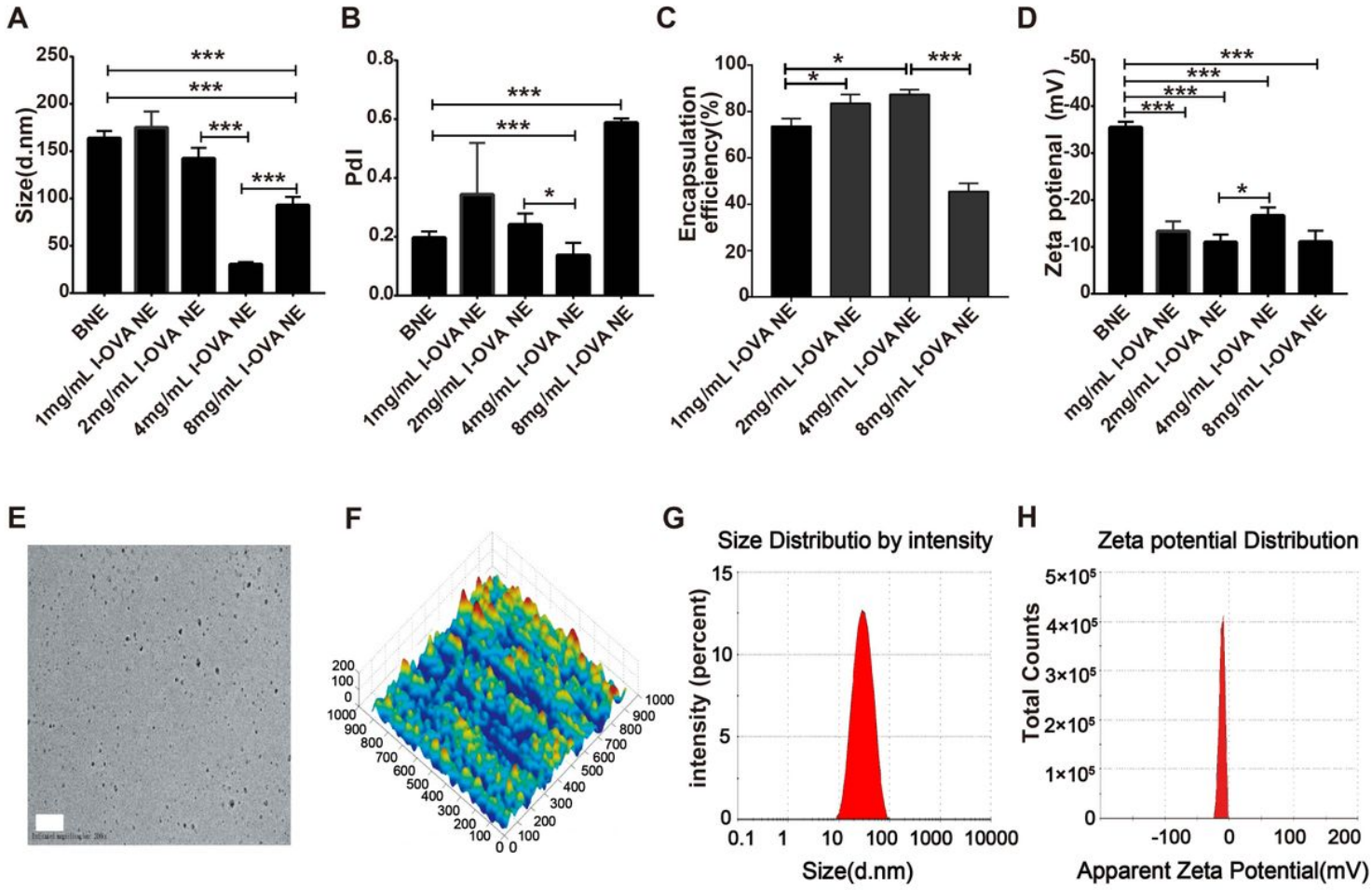

Figure 2

The optimized prescription and physical characteristics of the I-OVA NE vaccine. A. Particle size effect of I-OVA. (B) Polydispersity index effect of I-OVA. (C) Zeta potential effect of I-OVA. (D) Encapsulation efficiency effect of I-OVA. (E) Transmission electron micrograph, scale bar =100 nm. (F) Atomic force microscopy micrograph, the X and Y axes total 800 nm in length. (G) Size diameter distribution. (H) Zeta potential distribution. The data are expressed as the mean ± SD (n = 3). *: P < 0.05; **: P < 0.01; ***: P < 0.001.

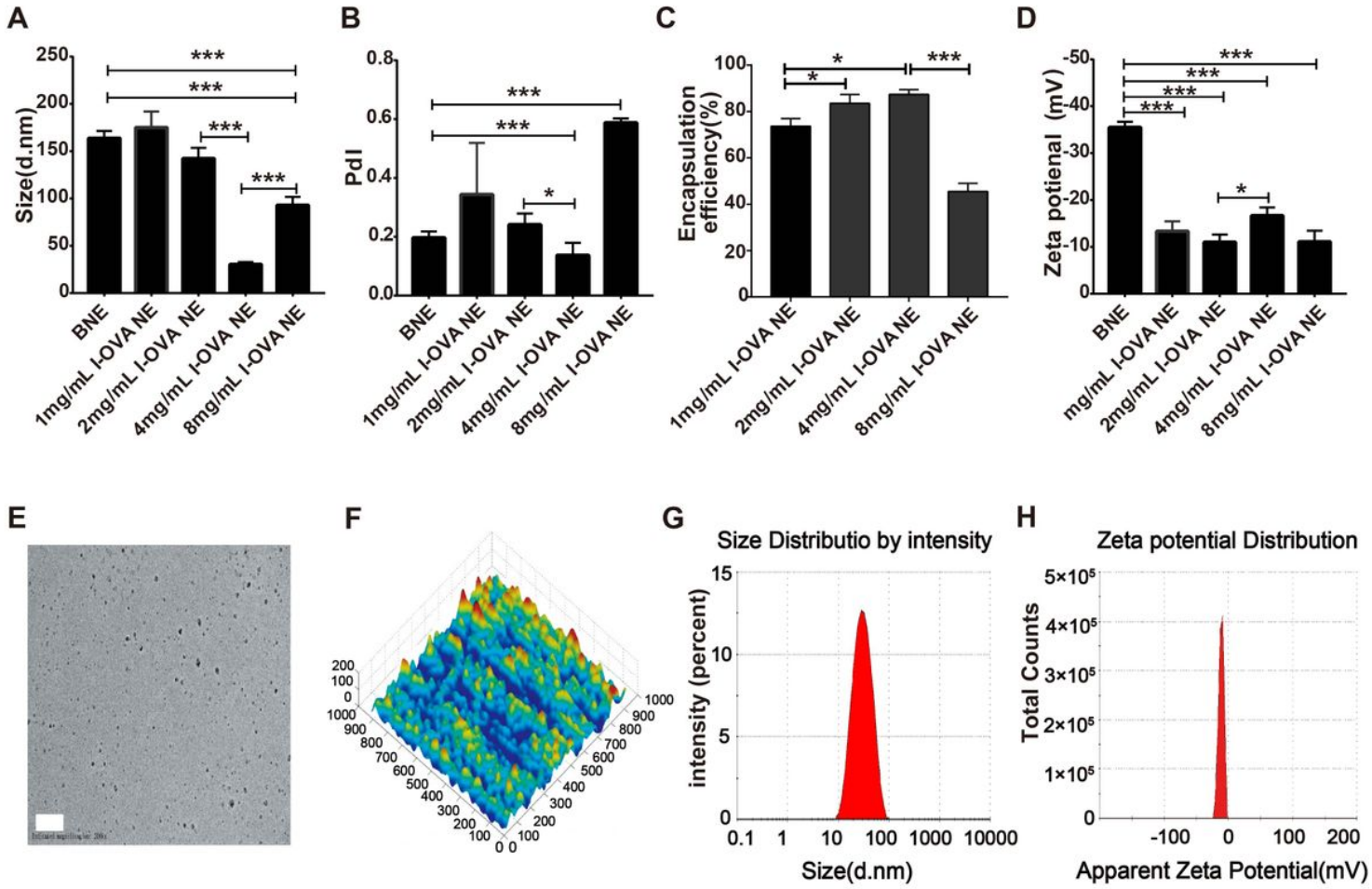

Figure 2

The optimized prescription and physical characteristics of the I-OVA NE vaccine. A. Particle size effect of I-OVA. (B) Polydispersity index effect of I-OVA. (C) Zeta potential effect of I-OVA. (D) Encapsulation efficiency effect of I-OVA. (E) Transmission electron micrograph, scale bar =100 nm. (F) Atomic force microscopy micrograph, the X and Y axes total 800 nm in length. (G) Size diameter distribution. (H) Zeta potential distribution. The data are expressed as the mean ± SD (n = 3). *: $P < 0.05$; **: $P < 0.01$; ***: $P < 0.001$.

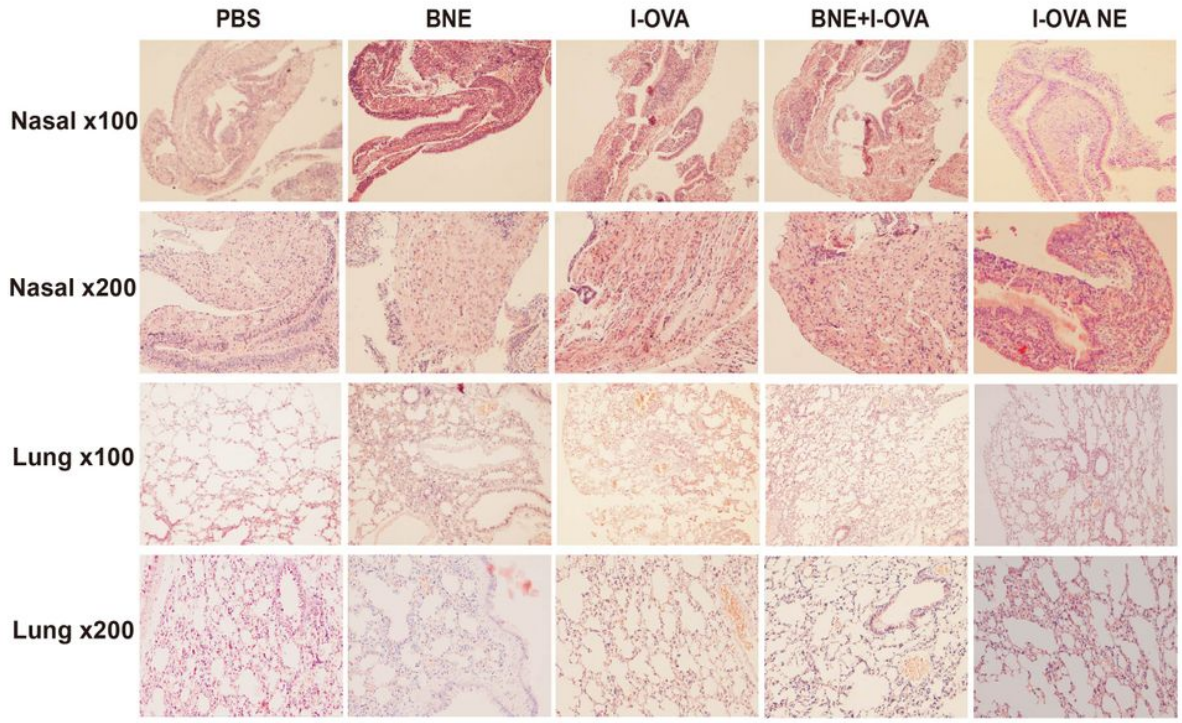

Figure 3

In vivo toxicology of the I-OVA NE vaccine. Microscopic examination of pathological sections of the nasal mucosa and lung tissues fixed 24 h after the challenge. Images were captured at 100× and 200× magnification. The data are expressed as the mean ± S.D. (n = 5). *: $P < 0.05$; **: $P < 0.01$; ***: $P < 0.001$.

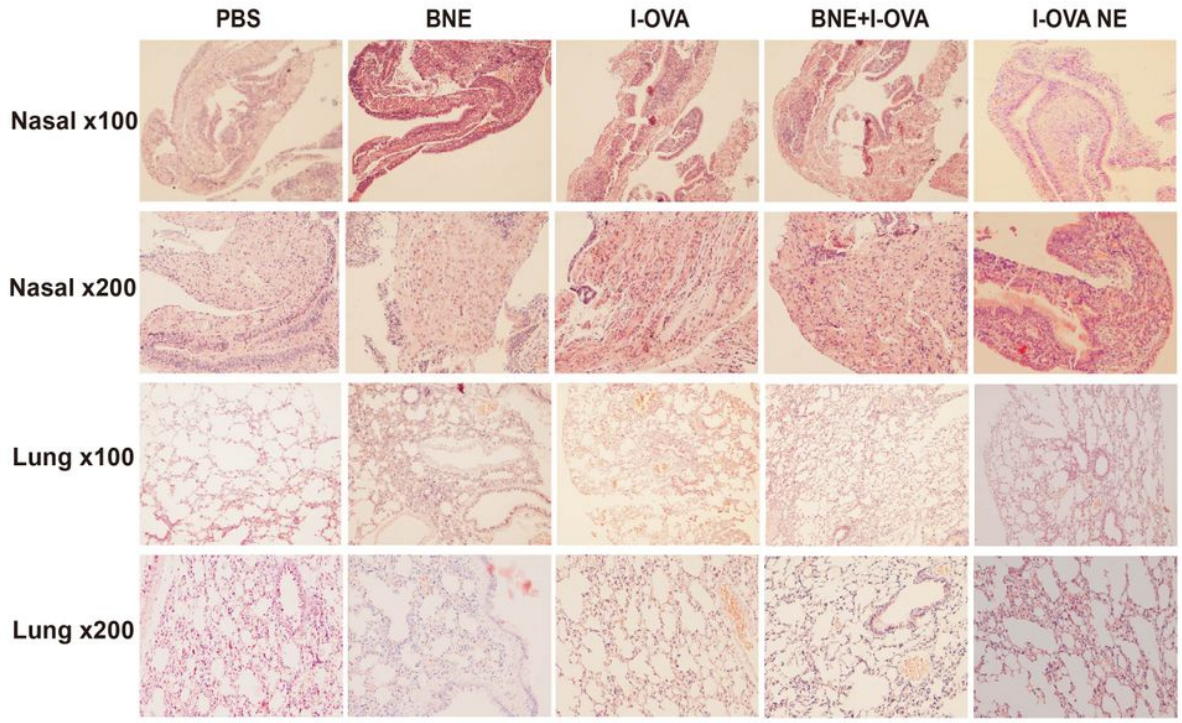

Figure 3

In vivo toxicology of the I-OVA NE vaccine. Microscopic examination of pathological sections of the nasal mucosa and lung tissues fixed 24 h after the challenge. Images were captured at 100× and 200× magnification. The data are expressed as the mean ± S.D. (n = 5). *: $P < 0.05$; **: $P < 0.01$; ***: $P < 0.001$.

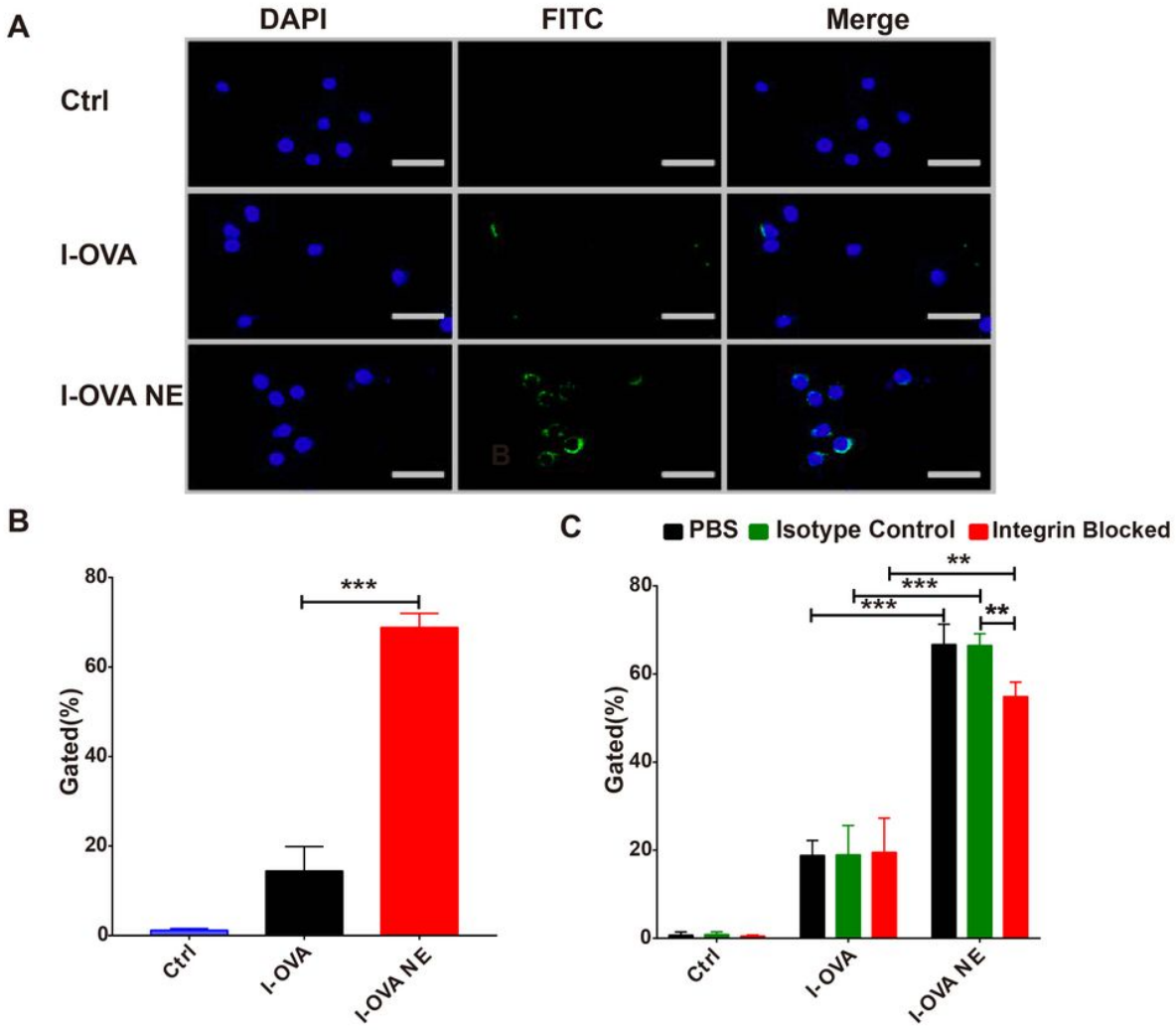

Figure 4

Cell uptake and antibody blockade of I-OVA NE. (A) In vitro confocal fluorescence imaging of BEAS-2B cells treated for 1.5 h with I-OVA or I-OVA NE. PBS was used as a control. I-OVA was labeled with FITC (green fluorescence), and nuclei were stained with DAPI (blue fluorescence) (Scale bar, 50 μm). (B) Uptake of FIT C-labeled I-OVA by BEAS-2B cells was analyzed using flow cytometry. (C) I-OVA NE uptake of BEAS-2B after integrin blockade. The data are expressed as the mean ± SD (n = 3). *: $P < 0.05$; **: $P < 0.01$; ***: $P < 0.001$.

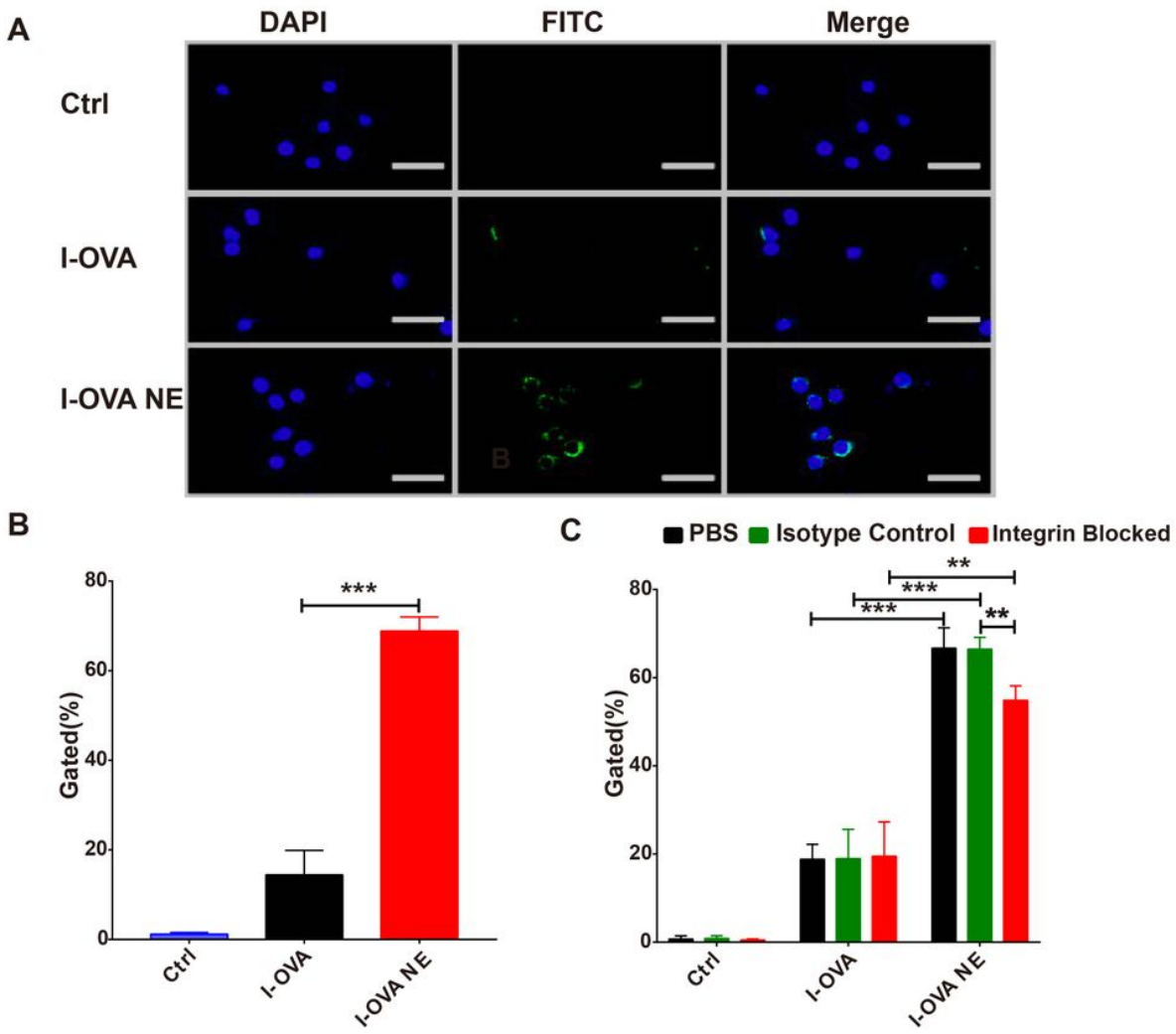

Figure 4

Cell uptake and antibody blockade of I-OVA NE. (A) In vitro confocal fluorescence imaging of BEAS-2B cells treated for 1.5 h with I-OVA or I-OVA NE. PBS was used as a control. I-OVA was labeled with FITC (green fluorescence), and nuclei were stained with DAPI (blue fluorescence) (Scale bar, 50 μm). (B) Uptake of FIT C-labeled I-OVA by BEAS-2B cells was analyzed using flow cytometry. (C) I-OVA NE uptake of BEAS-2B after integrin blockade. The data are expressed as the mean ± SD (n = 3). *: $P < 0.05$; **: $P < 0.01$; ***: $P < 0.001$.

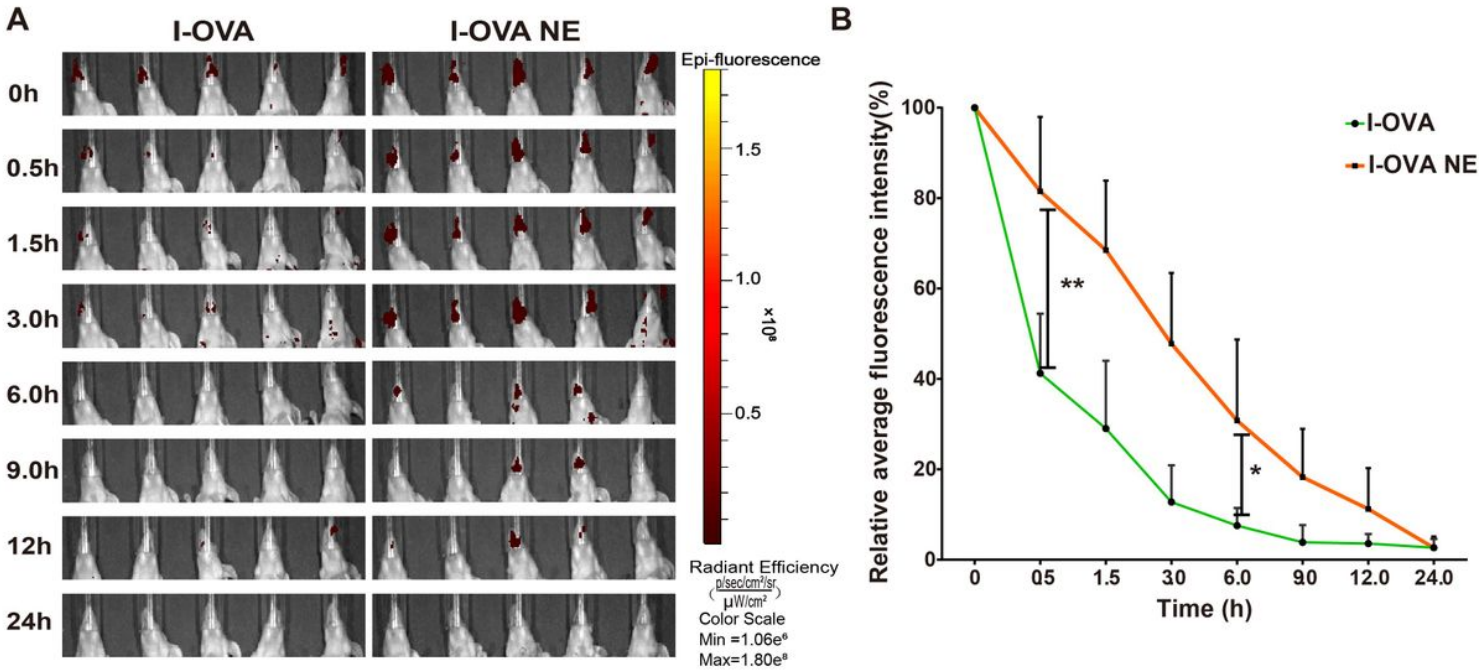

Figure 5

In vitro release of I-OVA NE. (A) In vivo fluorescence imaging of PE labeled I-OVA in the mouse nasal cavity. Relative fluorescence intensity recorded at 0, 0.5, 1.5, 3, 6, 9, 12, and 24 h after nasal administration of I-OVA or I-OVA NE. (B) Quantitation of fluorescence intensity. The data are expressed as the mean ± SD (n = 5). *: P < 0.05; **: P < 0.01; ***: P < 0.001.

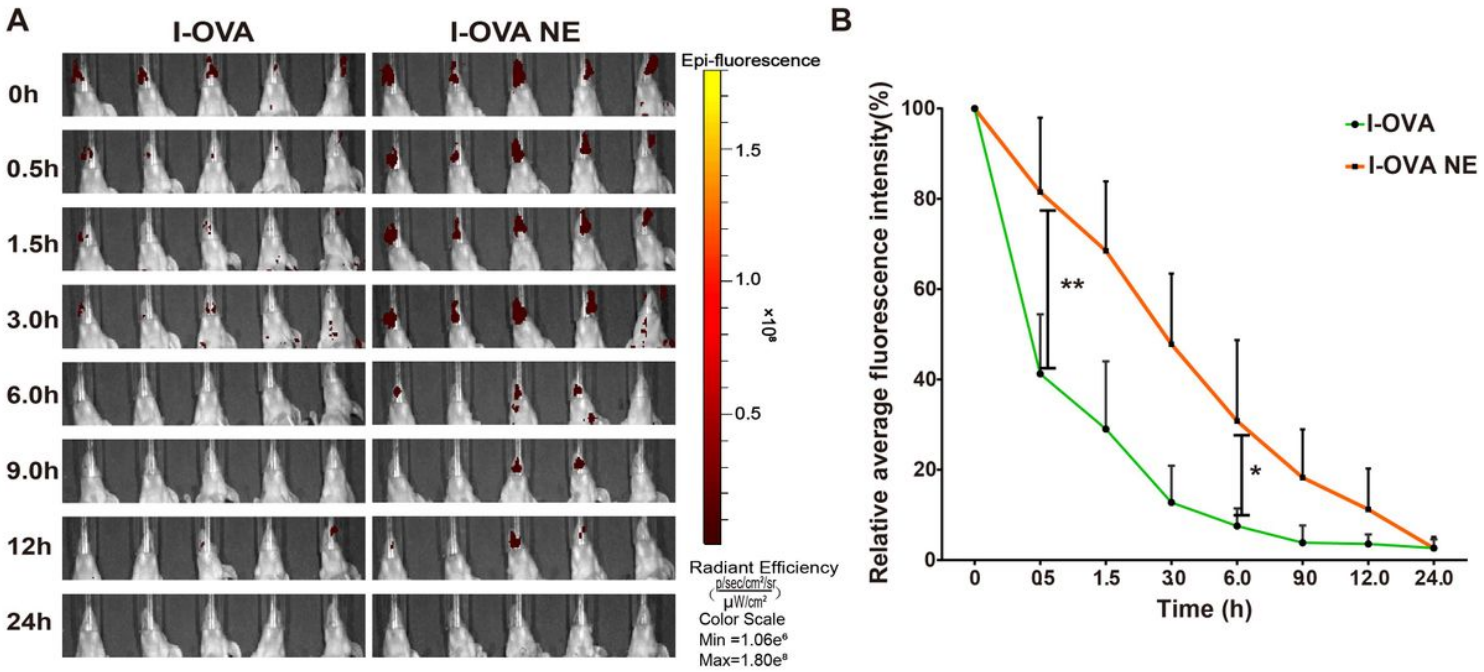

Figure 5

In vitro release of I-OVA NE. (A) In vivo fluorescence imaging of PE labeled I-OVA in the mouse nasal cavity. Relative fluorescence intensity recorded at 0, 0.5, 1.5, 3, 6, 9, 12, and 24 h after nasal administration of I-OVA or I-OVA NE. (B) Quantitation of fluorescence intensity. The data are expressed as the mean ± SD (n = 5). *: P < 0.05; **: P < 0.01; ***: P < 0.001.

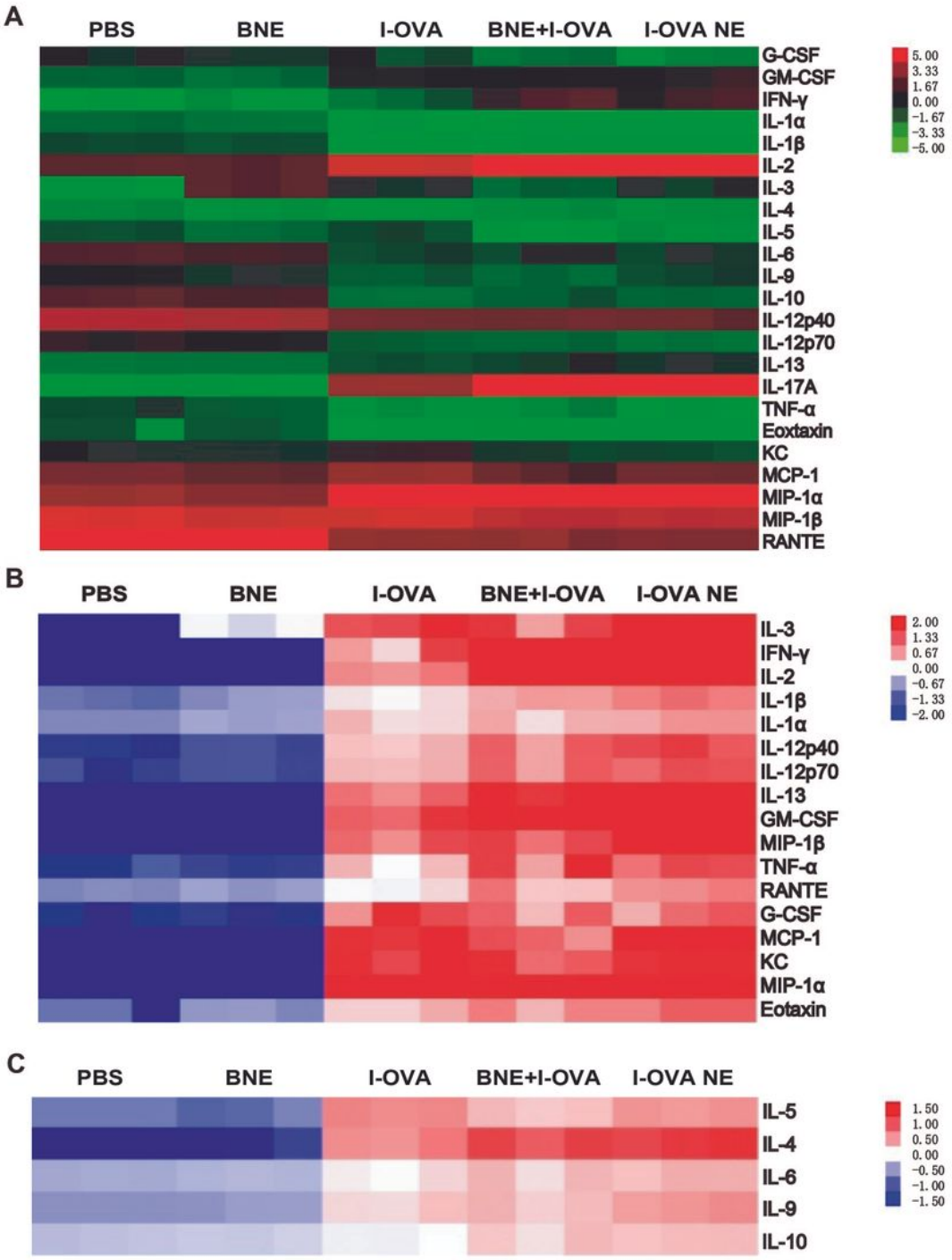

Figure 6

Heat map displaying the five group changes in the immune response. A. Each cytokine, B. Th1 immune response. C. Th2 immune response.

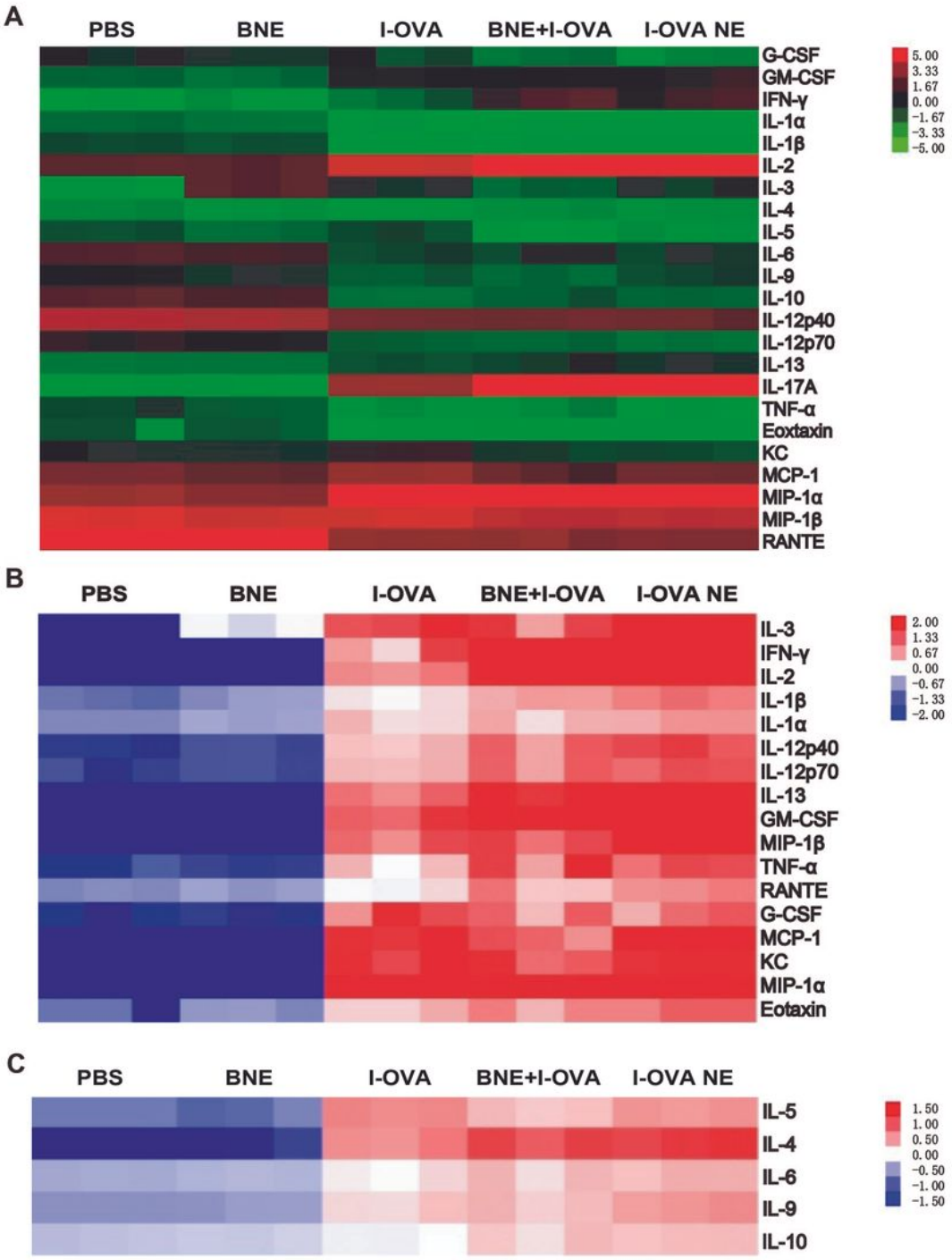

Figure 6

Heat map displaying the five group changes in the immune response. A. Each cytokine, B. Th1 immune response. C. Th2 immune response.

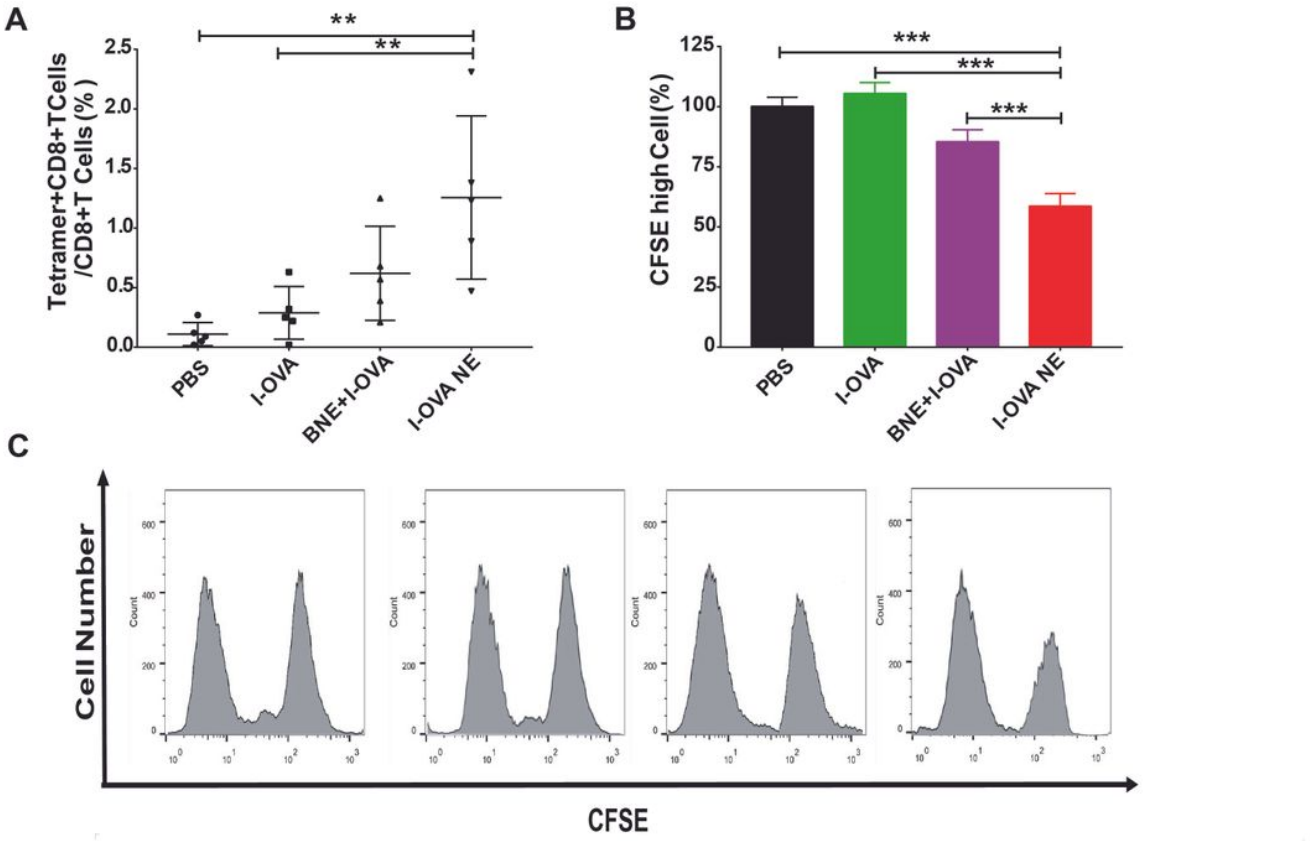

Figure 7

I-OVA NE-specific CD8+ T cells and in vitro CTL activity assays were measured after immunization. (A) The ratio of I-OVA NE-specific CD8+ T cells. (B) The ratio of CFSEhigh cells. (C) Typical flow cytometry graph. The data are expressed as the mean ± SD (n = 8). *: P < 0.05; **: P < 0.01; ***: P < 0.001.

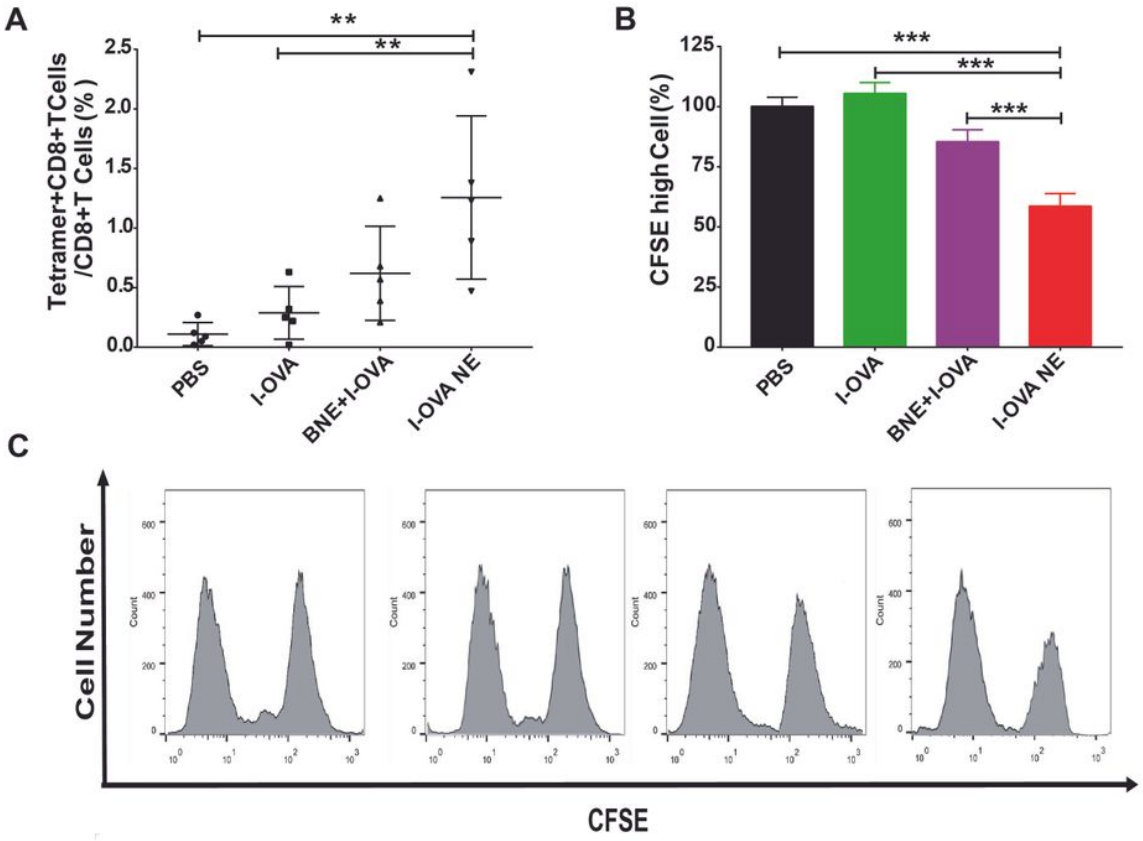

Figure 7

I-OVA NE-specific CD8+ T cells and in vitro CTL activity assays were measured after immunization. (A) The ratio of I-OVA NE-specific CD8+ T cells. (B) The ratio of CFSEhigh cells. (C) Typical flow cytometry graph. The data are expressed as the mean ± SD (n = 8). *: $P < 0.05$; **: $P < 0.01$; ***: $P < 0.001$.

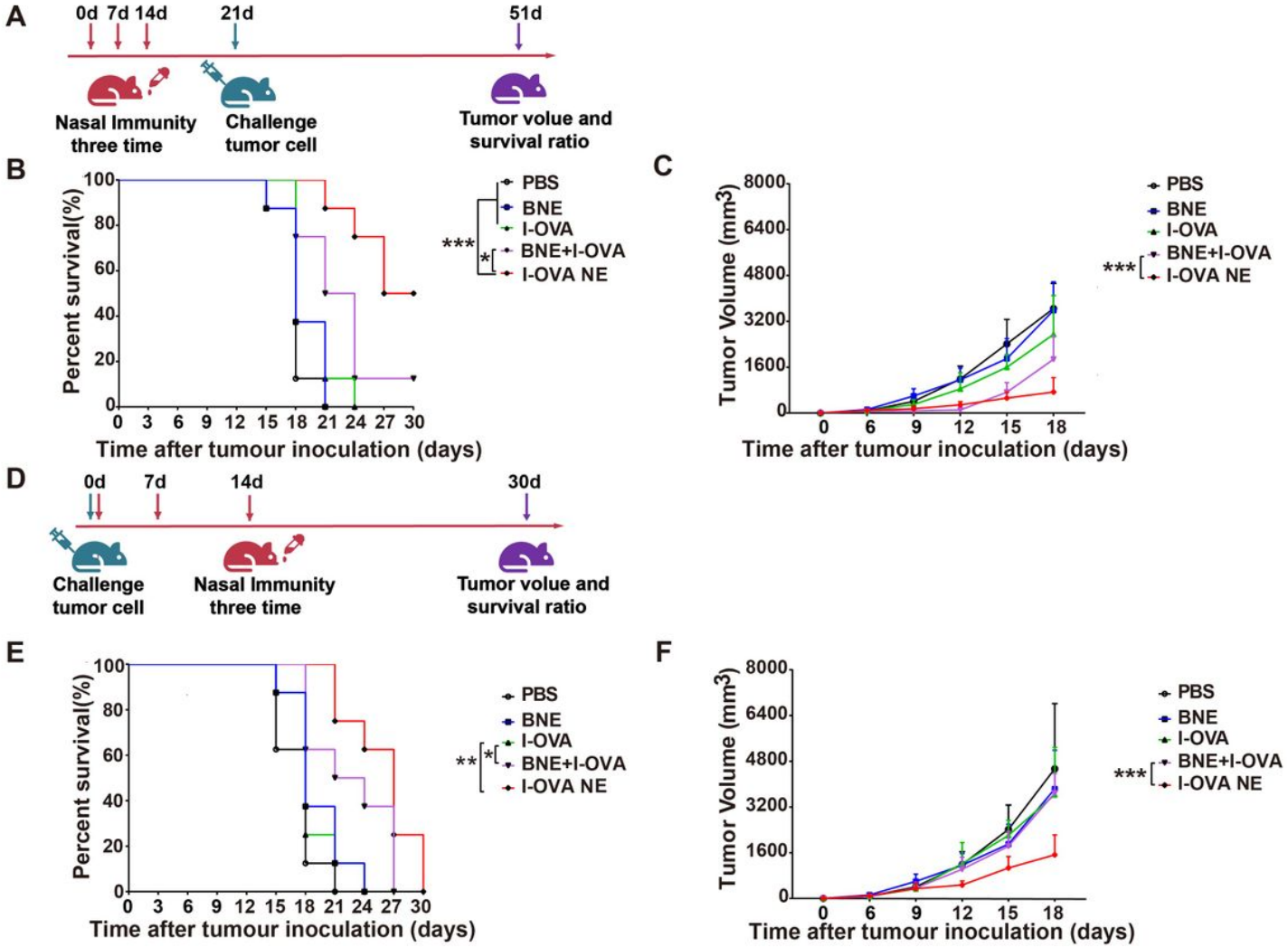

Figure 8

The preventive and therapeutic protective effect of I-OVA NE. (A) Animal treatment procedure of preventive effect. (B) Average tumor growth curves of the preventive mice. (C) Percent survival rate of the preventive mice. (D) Animal treatment procedure of therapeutic effect. (E) Average tumor growth curves of the therapeutic mice. (F) Percent survival rate of the therapeutic mice. *: $P < 0.05$; **: $P < 0.01$; ***: $P < 0.001$.

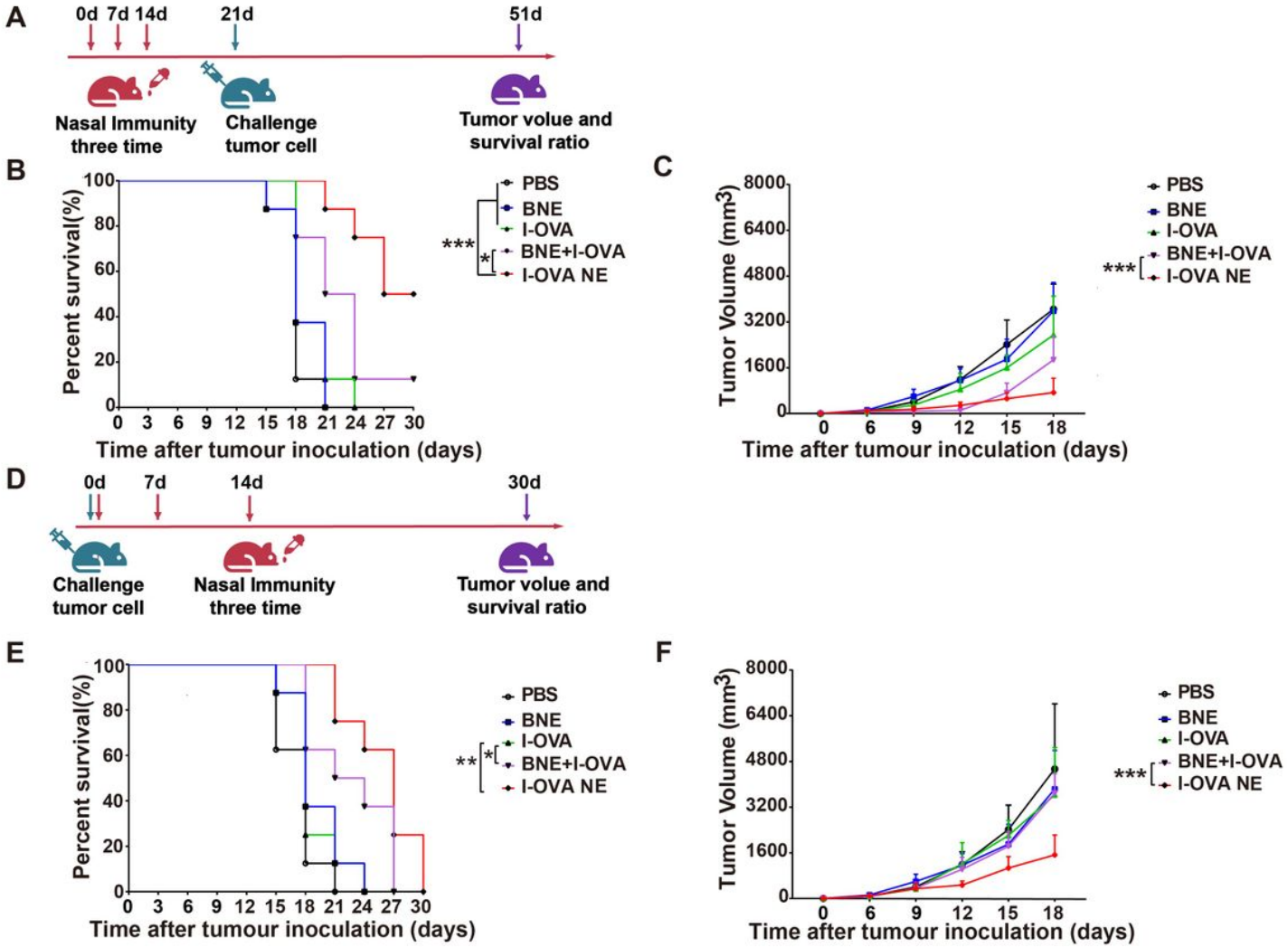

Figure 8

The preventive and therapeutic protective effect of I-OVA NE. (A) Animal treatment procedure of preventive effect. (B) Average tumor growth curves of the preventive mice. (C) Percent survival rate of the preventive mice. (D) Animal treatment procedure of therapeutic effect. (E) Average tumor growth curves of the therapeutic mice. (F) Percent survival rate of the therapeutic mice. *: $P < 0.05$; **: $P < 0.01$; ***: $P < 0.001$.

Supplementary Files

This is a list of supplementary files associated with this preprint. Click to download.

- renamed7aef7.doc
- renamed7aef7.doc